Lawrence Berkeley Laboratory
UNIVERSITY OF CALIFORNIA

Accelerator & Fusion Research Division

To be submitted for publication

A METAL VAPOR VACUUM ARC ION SOURCE

I.G. Brown, J.E. Galvin, B.F. Gavin,
and R.A. MacGill

August 1985

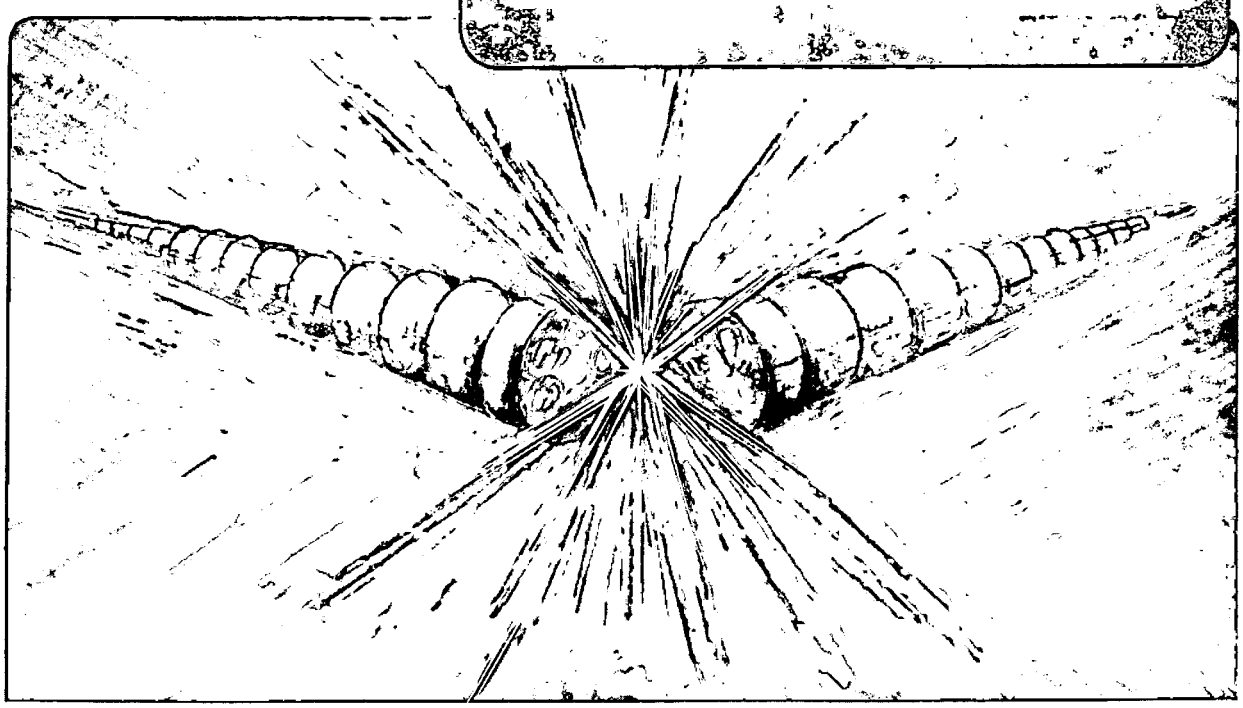

Prepared for the U.S. Department of Energy under Contract DE-AC03-76SF00098

DISCLAIMER

LBL-19976

A Metal Vapor Vacuum Arc Ion Source*

I. G. Brown, J. E. Galvin, B. F. Gavin, and R. A. MacGill

University of California
Lawrence Berkeley Laboratory
Berkeley, California 94720

August 1985

Abstract:

A high current ion source is described in which a metal vapor vacuum arc is used to create the plasma from which the ion beam is extracted. An ion beam current of up to about 1 Ampere has been measured, at an extraction voltage of 25kV, for a range of metallic species spanning the periodic table from lithium to uranium. Multiply ionized charge states are seen, up to as high as Q = 6+ in the case of uranium. In the metal vapor vacuum arc, regions of intense current concentration are formed at the cathode, and it is at these regions - the cathode spots - that the cathode material is vaporized and ionized to form a dense, quasi-neutral plasma which plumes away from the cathode surface. The plasma plume is caused to impinge upon a set of extractor grids, and the ion beam is extracted from the streaming metal plasma. A preliminary survey of the performance of the source has been made. We describe here the principle of operation of the source, the source design, and the results of those measurements that we have made to-date.

I. Introduction

The production of intense ion beams is a field that has assumed increasing importance over the last decade or so as the needs of research and industry have grown. As a result, some remarkable progress in ion source technology has been made. Thus for example the controlled fusion research program has called for intense neutral beams of hydrogen isotopes for heating and fueling the fusion plasma, in response to which need sources have been made that can produce beam currents of 70 Amps at 120 kV in several-second pulses[1,2]. Similarly, the heavy ion fusion research program has fostered the development of short-pulse beams of extremely high current; pulsed ion diodes have been used to create beams with currents approaching 10^6 Amps at energies exceeding 1 MV in pulse lengths from 10^{-8} to 10^{-6} seconds[3-7]. In the semiconductor industry there is a need for stable, well-controlled, dc beams for ion implantation of silicon wafers, and high quality beams of species such as boron, phosphorous, arsenic and antimony of up to 10 ma or so on target have been developed[8]. Finally, the emerging field of metallurgical surface modification and the production of exotic surface alloys is creating a need for intense ion beams of various species[9-11].

While the development of sources for gaseous ion species has been impressive, techniques for the production of metallic ion beams have not made similar advances. These kinds of sources have to-date employed vaporization of the solid material[12-15], or surface ionization[12,16-18], or sputtering[12,19,20], and beams of up to several

*This work was supported by the Director, Office of Energy Research, Office of High Energy and Nuclear Physics, Nuclear Science Division, U.S. Department of Energy, under contract number DE-AC03-76SF00098.

tens of milliamperes of metal ions have been obtained on a long-pulse or dc basis. The source that we describe in this paper makes use of another mechanism for establishing the metallic ion plasma from which the beam is to be extracted - this is the metal vapor vacuum arc.

The study of metal vapor vacuum arc plasma discharges - also called vacuum arcs, or metal vapor arcs - had its origin in the high power switching field, and research in this discipline has remained overwhelmingly the province of the high power electrical engineering community. The metal vapor arc provides a means of switching high current at high voltage in a vacuum environment - this is the vacuum switch, invented by R. A. Millikan and R. W. Sorensen. One of the earliest publications on this work is that of Sorensen and Mendenhall in 1926[21], and a historical survey of this field, pre-1960's, has been given by Cobine[22]. More recently, a very complete review of the entire field has been given by Lafferty[23].

A closely related plasma discharge - the vacuum spark - is fairly-well developed and has been used as a spectral source[24,25] and ion source[26,27] for some time. Characteristic of vacuum sparks is the production of very highly stripped species of the electrode material, and the helium-like spectral lines Ti^{20+}, Fe^{24+}, and Co^{27+}, for example, have been observed[25]. These sources are however inherently of sub-microsecond duration.

The production of ions by the metal vapor vacuum arc plasma has been investigated by a number of authors for at least the last two decades[28-37]. One of the earliest attempts to incorporate the arc as the method of plasma production for use as an ion source is the work done as part of the Manhattan Project in World War II; however, this source suffered from several drawbacks and was not pursued[38]. Revutskii et

al[39], in 1968, investigated a cylindrically symetric arc geometry; their configuration employed ion extraction through a hole in the cathode, (as opposed to through the anode as in our work, to be described), and their work appears not to have been pursued. More recently, significant progress has been made by Coffey et al[40], Burkhart et al[41], and by Adler and Picraux[42].

The embodiment of the concept that we've developed makes use of a coaxial configuration of the arc in which a portion of the arc plasma is allowed to flow through a central hole in the anode. This arc geometry has been studied by Gilmour and Lockwood[43], and we have drawn extensively upon their work. The coaxial metal plasma generator thus produces a plume of plasma expanding into the vacuum and away from the arc itself. It is this plasma plume that we have used as the medium from which ions are extracted to form an intense beam of metal ions. A summary of our source and some results has been presented previously[44,45]. In this paper we describe the source in detail and present the full array of our experimental findings.

II. Source Design

The METal Vapor Vacuum Arc (MEVVA) ion source is composed of a metal vapor vacuum arc plasma source, a drift space or plasma shaping region, and a set of grids for ion extraction. The structure is housed within a simple vacuum chamber having a base pressure in the 10^{-6} torr range. An outline of the source is shown in Figure 1.

A characteristic of the metal vapor arc discharge is the formation of cathode spots on the cathode surface. These are minute regions of intense current concentration, and have been the focus of much research over many years[28-37,46,47]. Although there is still conflicting opinion as to the

details of the physics of arc and cathode spot formation and behavior, there is general agreement that at the cathode spots the current density is of rough order 10^6 Amps/cm^2, and that this current serves to vaporize and ionize the cathode material within the spots. Thus the cathode spots act as small regions of plasma generation from the solid surface. Multitudinous spots form, generally, and the assemblage of such spots constitutes a source of metal plasma produced from the cathode material. This quasi-neutral plasma plumes away from the cathode toward the anode, and persists for the duration of the arc. One should note that it is also possible for spots to form on the anode[47-49], which we would like to avoid; this discharge mode seems to be confined to higher arc current than we have used here and thus presents us with no problem.

The anode is an annular disk some several centimeters away from the cathode, with a central hole of diameter approximately 1cm. The electrical circuit necessary to maintain the arc is completed by current flow (mainly electron current) from cathode to anode and the arc persists for as long as the external current drive is on. Some of the plasma flows through the hole in the center of the anode, and it is this component of the plasma that forms the medium from which ions are extracted. This plasma plume drifts through the post-anode region to the set of grids that comprise the ion extractor.

The ion extraction system consists of a set of three grids. Each grid is an array of about 100 or more small holes of diameter about 1mm or so, with an array diameter of 2cm. Thus the initial beam size is 2cm diameter. The hole pattern is well aligned grid-to-grid. We've experimented with various grid geometries and the final configuration is the result of an approximate optimization of beam current, beam divergence, and voltage hold-off. The first grid (closest to the anode)

is connected to the anode through a 500 Ω resistor - an empirical adjustment that we found to be insensitive. The second (middle) grid is the electron suppressor and is held at approximately -1 kV; this prevents the flow of secondary electrons, created by and residing in the ion beam, back across the accelerating gap and thus contributing to the load on the extractor power supply, as well as possibly causing breakdown across the gap. The third (outermost) grid is tied to ground. The arc (cathode-anode circuit) and the first grid are held at extractor voltage, which for the work described here has been mostly in the range 10 to 25 kV. The ion accelerating voltage is thus applied across the gap between grids one and two. The physics of ion extraction and beam formation using this kind of grid system is well understood and has been described by a number of authors[50-53].

The main arc is initiated by a trigger spark discharge between the cathode and a coaxial trigger electrode which is separated from the cathode by a close-fitting, thin wall alumina tube. A short pulse of several microseconds duration and of amplitude 10 - 20 kV serves to generate a small amount of plasma which allows current flow to the anode and consequent evolution of the main arc circuit. The triggering and formative phase of a vacuum gap is a very different phenomenon to the more usual situation of gaseous breakdown. In the latter case the current-carrying plasma grows through an electron avalanche in the ambient gas, in which ionization of gas atoms by electron impact is the pertinent process allowing growth of the arc[54]. The processes involved in the breakdown and plasma growth of the metal vapor vacuum arc discharge are poorly understood. It seems, however, that it is necessary to establish, through the trigger spark, one or more cathode spots on the cathode

surface in order for the arc to grow[22,55-60]. We have tried various trigger electrode - cathode geometries, and that configuration which performs best under our conditions is a central cathode with a coaxial trigger electrode surrounding the cathode and separated from it by the alumina insulator, as opposed to a central trigger with coaxial cathode.

A magnetic field is established throughout the arc and plume region by a coil located at the anode plane[43]. The dc field strength can be varied from zero to several hundred gauss. This field serves to confine the arc radially and thus to channel a high fraction of the arc plasma through the central hole in the anode, and to guide the streaming plasma plume from anode hole to extractor. In this manner the efficiency with which cathode material is transformed into useable ion beam is maximized. The magnetic field also adds an additional control over the plasma density and radial profile at the extractor, thus helping to optimize the extraction optics and consequent beam quality. It is also possible that the magnetic field helps to suppress the growth of magnetohydrodynamic instabilities in the arc plasma, by virtue of the favorable field curvature[61-63]; this would result in a more quiescent extracted beam than might otherwise be possible. However, the magnetic field is not an essential ingredient to the concept, and we have often operated with the magnet switched off.

We have constructed and tested several versions of the MEVVA ion source. Figure 1 shows the essential features, and is a drawing of our MEVVA II version; Figure 2 shows the disassembled MEVVA II. We constructed a small version, MEVVA III, and a photograph of this embodiment is shown in Figure 3.

III. Experimental Setup

We describe here the experimental facilities that we have used to survey the MEVVA ion source performance. These include the test stands, the support electronics, and the diagnostics used to monitor the beam.

Much of our work has been carried out using the MEVVA II source attached to and injecting into a 120 cm long, 60 cm diameter vacuum chamber which was pumped to a pressure in the 10^{-6} torr range. Visual and diagnostic access to the source and beam was possible through a number of vacuum ports. The region of beam propagation was magnetic-field-free, and electrons necessary for space charge neutralization of the ion beam are free to flow along and across the beam as needed to provide neutralization. Appended to the vacuum chamber is a 180 cm long, 20 cm diameter cylindrical extension, which serves as our time-of-flight charge state analysis diagnostic.

Another test-stand was equipped with a very large volume, uniform magnetic field pervading the entire vacuum region. The MEVVA II source could be located just outside the field region with the beam injecting into the transverse magnetic field. Magnetic charge state analysis was possible by measuring the current collected by a Faraday cup located in the field volume and scanning either the cup position or the field strength.

The arc power supply was a simple pulse line. The line is a 6-section LC network of impedance 0.5 Ω and pulse length 300 μseconds, with a modified Gibbs section on the front end to provide a fast rise to the pulse. The line is charged to a voltage of several hundred volts with a small dc power supply, and the output is connected to the anode and cathode terminals of the source. When the triggering pulse is applied to

the trigger electrode, the cathode-anode circuit is closed by plasma and the arc proceeds. The trigger pulse is the discharge of a 0.1 μF capacitor at up to 5 kV, switched using a 5C22 thyratron, through a step-up isolation transformer the output of which is connected trigger-to-cathode. The trigger voltage obtained in this way is 10-20 kV and of several microseconds duration, with the trigger positive with respect to cathode. The ion source repetition rate is determined by the trigger pulse and is limited by the charging times of arc and trigger circuitry and by average power constraints on various components. For most of our work we've run at several pulses per second; the maximum repetition rate was 10 pps and this was electronics limited. We have also run with arc and extracted beam pulse width of up to 3 msec; and we've run the arc alone for as long as 20 seconds, using a dc power supply and without extracting beam. A schematic outline of the source circuitry in its 'usual' configuration is shown in Figure 4.

We have looked at the behavior of the three main components of the device - the arc, the plasma plume, and the extracted ion beam. The arc voltage and current were monitored quite conventionally. A framing camera with microsecond exposure time[64] allowed a visual recording of the growth and decay of the arc. The metal vapor plasma plume was monitored using a gridded, electrostatic energy analyzer[65-69], with Langmuir probes[70], by measuring the mass deposited on a collector plate, and photographically. Properties of the extracted ion beam were measured using: Faraday cups of several different designs; calorimeters of several different designs; a 16-channel beam profile monitor; a thin foil target to observe target incandescence (beam energy) and motion (beam momentum); visual photography. The charge state distribution of ions in the

extracted beam was determined with a time-of-flight diagnostic of quite conventional design. We've also used magnetic charge-state analysis of the beam but we have yet to arrive at a transport geometry that is optimum and hence the magnetic analysis studies have been plagued by loss of a considerable fraction of the beam between source and Faraday cup, and poor focussing of beam at the detector. None-the-less, the magnetic analysis has provided confirmation of the charge state distribution for those cases at which we've looked. Beam transport - quadrupole focussing and dipole analysis - constitutes our current effort.

IV. Source Performance

We describe here first some general observations of the source behavior, and then in turn characteristics related to the arc, the plasma plume, and the extracted ion beam.

A. General Operating Conditions

(i) Cathode Material

For accelerator application at Lawrence Berkeley Laboratory the main interest is in producing intense uranium beams in the SuperHILAC (8.5 MeV/amu) and the Bevalac (~1 GeV/amu)[71-74]. We've operated the MEVVA source using a cathode fabricated from depleted uranium (99.9% U^{238}), but for ease of handling most of our work has been done using tantalum. Other elements are of interest also, and we've produced beams of hundreds of milliamperes from the following range of materials: lithium, boron, carbon, aluminum, silicon, titanium, iron, cobalt, nickel, copper, niobium, lanthanum, tantalum, gold, lead and uranium. The boron and lanthanum were produced from a lanthanum hexaboride cathode, which is of

some interest since it implies that non-metallic elements can be ionized and extracted by incorporating them into a cathode as a conducting compound. This might also hold for alloyed materials, but we haven't looked at this yet.

(ii) Triggering

We've tried a number of different trigger configurations, including geometries in which the trigger is a central pin within the cathode, and alternatively in which the trigger is an annular ring surrounding the cathode. Our prefered configuration at the present is the latter geometry. With the central trigger pin the failure mode is a gradual plating over of the alumina sheath which insulates the trigger from the cathode with cathode material, eventually producing a short and a failure to trigger. Under typical operating conditions we might obtain 300,000 triggerings before failure. The annular trigger, on the other hand, has run for in excess of 700,000 shots without failure. In this case there seems to be no deterioration of the trigger-cathode insulator, and the dominant evidence of age is removal of cathode material by the arc.

(iii) Source Conditioning

As with most ion sources that employ an extractor at high voltage, it is necessary to "bake-in" the source first, in a special conditioning run, in order to obtain maximum voltage holding capability[2]. Usually breakdown occurs between the first and second grids, across which the full extractor voltage is applied. The bake-in procedure is to let the source operate at a few pulses per second for a period of a few minutes up to a few hours, as necessary, while gradually raising the arc current and the

extractor voltage. In this way the plasma density is increased along with the extractor voltage, as is necessary for optimal extraction optics. When the grids are conditioned in this way they will hold voltage indefinitely, requiring only minimal re-conditioning after exposure to air or after handling. Maximum extraction voltage at which we've run to-date is about 30 kV, with an extraction gap (grid one to grid two) of 1.7mm. This voltage was power-supply-limited, and we are constructing a new extractor supply with which we will be able to run at voltages up to 60 kV.

B. The Arc

After initiation by the trigger-to-cathode spark discharge, the vacuum arc proceeds for the duration of the current supply - the pulse line for these experiments. The anode-cathode voltage, which before breakdown was equal to the pulse line charging voltage, drops within a few microseconds to a lower level called the arc drop or the arc burning voltage. The arc drop depends on the cathode material and on the arc current, and is lower for lower Z materials and for lower currents. For carbon the arc drop may be in the vicinity of 20 volts, while for uranium it may be closer to 100 volts. In all cases, there is a good correlation between arc voltage and the ionization potential of the most highly stripped state seen in the charge state spectrum. Typically the arc resistance (ratio of arc voltage to arc current) is a few hundred milliohms or less. An oscillogram of arc voltage and current for the case of a cobalt cathode is shown in Figure 5.

Cathode spots are clearly visible with ordinary photography, either time integrated or using a framing camera of some microseconds exposure

time. A series of such framing camera photographs is shown in Figure 6. These are pictures of the cathode of the MEVVA I source taken at a sequence of times throughout the arc pulse. Each photograph was taken on a different discharge; the whole sequence does not correspond to a single arc discharge. The exposure time was 8 μseconds. In this case the trigger electrode is coaxially surrounding the cathode, and the spots tend to congregate around the outer circumference of the cathode. There are up to only a dozen or so spots at any one time, during the main part of the arc, and the spot number and intensity seems to follow the arc current pulse shape.

The size of the anode hole was chosen as a compromise: one would like a large aperture to maximize the fraction of the arc plasma that plumes through the hole and into the drift region beyond, but on the other hand plasma must flow to the anode in order to allow the arc current to flow. We have observed that the arc will not trigger when the anode hole size and the anode-cathode spacing are such that the 'magnetic shadow' of the cathode at the anode is smaller than the anode hole. In this case, electrons and plasma generated by the trigger spark at the cathode are ducted along magnetic field lines from the cathode towards the anode, but pass through the anode hole. In the MEVVA I source configuration, it was possible to vary the anode-cathode separation via a vacuum feedthrough arrangement, while running, and one could readily move between these two regions (arcing or non-arcing). The flux conservation rule is Br^2 = constant, and this precisely defined the maximum separation:

$$r_a = \left(\frac{B_c}{B_a}\right)^{\frac{1}{2}} r_c, \qquad (1)$$

where r_a is the radius of the anode hole, r_c the cathode radius, B_a the magnetic field strength on axis at the anode plane and B_c the magnetic field strength on axis at the location of the cathode.

C. The Plasma Plume

A bright and well-collimated plasma plume is generated by that part of the arc plasma that flows through the anode hole. A photograph of this plume is shown in Figure 7; this is uranium plasma in MEVVA I. The anode is on the left and the extractor on the right hand side of the photograph. The apparent blow-up of the plasma is not a space-charge effect, as the plasma plume is approximately charge-neutral, but is due to the flow of plasma along the magnetic field lines. The shape of the bright region in the photograph closely follows the flux conservation rule Br^2 = constant.

A thin metal target plate (piece of aluminum foil) was located some distance from the anode in such a manner as to collect the mass of tantalum transferred away from the arc by the plasma plume. In this case no extractor grids were used - simply the 'plasma gun'. The mass of the foil was measured before and after a series of several hundred shots. The arc charge transfer per shot, $\int idt$, was 0.13 Coulomb (440 amps for 300 μsec) and the plume mass deposition was 0.53 μgm/shot. This is a specific mass transfer of 4×10^{-9} Kgm/Coulomb of arc current. Note that this refers not to the total mass evolved from the cathode but just to that component that streams through the anode hole and is thus available to the extraction grids for the creation of beam. This value is only about 5% of the total cathode mass evolution, in the form of ions, as estimated by previous workers[31,43], and might be taken as an indication of the efficiency with which the plume transfers mass out of the arc for

the geometry of the MEVVA I source; one might speculate that an improvement in this efficiency might be possible, of perhaps up to near an order of magnitude, by judicious choice of geometry. It is interesting to note that the measured mass transfer implies a maximum ion current,

$$i = m\bar{Q}e/m_{ion}t, \qquad (2)$$

where m is the mass transfer per shot, $\bar{Q}e$ the mean charge per ion, m_{ion} the mass of a tantalum ion and t the pulse duration. For the above experiment, and taking $\bar{Q} = 3.5$ as measured (to be described), we obtain i = 3.3 amperes, averaged over the pulse length. Considering that the extractor does not span the entire plume diameter and that the grids are only 77% transparent, this estimate of maximum beam current is in surprisingly good agreement with that measured, about 1 Ampere peak.

We have measured the temperature of the ion component of the plasma plume using a gridded electrostatic energy analyzer[67,68] located some distance from the anode. If the analyzer was positioned too close to the source the thin grids would heat to incandescence and burn; thus it was necessary to sample at a distance, where the plasma flux density had fallen to a lower level because of the fall-off in magnetic field strength. The results of a typical measurement are shown in Figure 8. For this data the current to the collector plate is measured as a function of collector plate voltage, with the first (outermost) grid of the analyzer grounded and the second grid (just in front of the collector plate) biased at -225V so as to repel the electron component of the plasma plume. Thus the collector current is predominantly ion current. In this case the ion current to the collector plate is given by

$$i(v) = e\bar{Q}nA\int_{v_{min}}^{\infty} vf(v)dv \qquad (3)$$

where $e\bar{Q}$ is the mean ion charge, n is the ion density in the plasma being sampled, A is the effective collection area of the analyzer, f(v) is the ion velocity distribution in the longitudinal direction (direction of plasma flow), and v_{min} is the minimum ion velocity accepted by the collector plate for a given collector bias,

$$\tfrac{1}{2}mv_{min}^2 = \bar{Q}e\,(\phi - \phi_{pl}) \qquad (4)$$

The derivative of equation (3) is proportional to the distribution function,

$$f(v) \propto \frac{di}{d\phi}\,, \qquad (5)$$

so long as $\phi > \phi_{pl}$.

Thus the shape of the parallel ion velocity distribution and the ion temperature (slope of the tail) can readily be determined. These results are shown in Figure 8. It can be seen that the distribution is approximately a shifted Maxwellian with a parallel ion temperature of 15 eV. We hesitate to ascribe absolute significance to the offset of the distribution because of unknown sheath potentials, but the fit to a Maxwellian temperature of 15 eV is good.

D. Ion Beam

(i) Beam Current

The main diagnostics used for measuring beam current were current collecting plates (i.e., simple Faraday cups) and calorimeters. Over the course of our work we've used a number of different embodiments of each. The Faraday cups have included biasing, biased grids, and a transverse magnetic field for electron current suppression. In all cases we would routinely check for adequate electron suppression by varying the cup bias

voltage over a wide range to verify that we were operating in a regime where the cup current is independent of cup voltage. The design that provided the most reliable operation (cup current independent of voltage over a wide range) was one in which a large permanent magnet was used to establish a transverse field volume at the collector plate and for some centimeters in front of it. A calorimeter can be used to measure beam power, and if the beam voltage is taken to be the extractor voltage then the current is determined; this is standard practice. We've used calorimeters in which the temperature rise of a thin copper foil target is measured by the change in resistance of a sensitive thermistor on a single-shot basis, and alternatively in which the temperature rise of a known flow of water is measured for the case when the beam is rapid-pulsed. Thus we have an accumulation of checks and cross-checks on the beam current measured by these diagnostics. There is agreement between the methods to within 10-20%.

The highest beam current that we've measured to-date is 1.1 Amps; this was for tantalum (all charge states) at an extraction voltage of 25 kV. We have also measured 0.5 Amps of niobium beam at 14 kV and 0.8 Amps of lithium at 17 kV. These data were taken under quite different operating conditions, and should not be compared quantitatively to each other. We may conclude, however, that a beam current of up to about 1 Ampere can be extracted.

An important diagnostic that we've developed is a 16-cup beam profile monitor[75]. This is a linear array of 16 current collecting plates, each 1.6 cm square, mounted individually on ceramic standoffs to a rigid metal strap positioned across a diameter perpendicular to the beam propagation direction. The detector spans a diameter of 27 cm and was

positioned 1m away from the ion source. Signals from the collector plates were fed into a simple computer data acquisition system that displayed the beam radial profile and an array of derived data on a monitor immediately following each shot[76]. The data obtained using this diagnostic show that the beam is in general well-fitted by a Gaussian profile, and the total beam current derived from the profile, $\int_0^\infty 2\pi r j(r) dr$, is in good agreement with total current measurements obtained with the Faraday cups and calorimeters.

As a further indication of beam current, a thin carbon foil (a stripper foil) was suspended in the beam path. This simple technique, though far from rigorous, provided a graphic visual confirmation of the high current beam. The foil was of thickness 5μgm/cm^2, and it was heated to white incandescence by a 200 μsec long beam pulse with 15 kV extraction voltage. A simple calculation using these values indicates that incandenscence should occur for a beam current density of 1 to 2 ma/cm^2 if a loss-free 'impulse' approximation is made, and completely fortuitously about the same beam current density is implied if a steady-state radiation-equilibrium approximation is made. This compares favorably with the measured value of about 2 to 3 ma/cm^2 obtained using the profile monitor. This observation thus provides yet further confirmation of our interpretation of beam current.

(ii) Beam Emittance

We have yet to carry out a detailed study of beam emittance using the traditional multi-aperture or scanned aperture techniques[12]. We have however made some measurements of the beam radial profile, which together with the known geometry of the configuration allow a simple

estimate to be made of the emittance.

Measurements were made of the radial profile as a function of distance of the profile monitor from the source. For each axial distance a Gaussian was fitted to the data and the half-width radius (HWHM) of the profile determined. This data is plotted in Figure 9. For this run the MEVVA II source was used with a tantalum cathode, with the extraction voltage being 15 kV. One can see: (a) the beam diverges linearly up to z $\simeq$ 60 cm; (b) the envelope extrapolates back closely to the radius of the extractor, 1cm; (c) the beam divergence half angle is 2.9°. Beyond z = 60 cm the fit of the beam profile to a Gaussian is not good; this effect may be partially instrumental. An approximation to the beam emittance is given by

$$\varepsilon = \pi R_o \theta \tag{6}$$

where R_o is the extractor radius and θ is the beam divergence; this assumes that the beam envelope is at a waist at the extractor, and this is an approximation of the present method. The normalized emittance is

$$\varepsilon_N = \beta\varepsilon = 1.4 \times 10^{-3} \left(\frac{\bar{Q}\, V'_{ext}}{A}\right)^{\frac{1}{2}} \cdot \pi R_o \theta \tag{7}$$

where $\beta = v/c$, $\bar{Q}$ is the mean charge state, V'_{ext} the extraction voltage in kV and A the ion mass in amu. For the data presented here, and taking $\bar{Q} \simeq 3$, the normalized emittance is $\varepsilon_N = 0.036\pi$ cm. mrad., measured to the beam HWHM. This is about the best emittance we've obtained, for an uncollimated beam.

The 16-cup beam profile monitor and associated computer data acquisition and analysis system provide an estimate of beam emittance on a single-shot basis. Figures 10 (a) and (b) show the beam profile and fitted Gaussian for the case of a high current beam and for a beam which has been collimated to tighten the emittance, (respectively). For Figure

10 (a) the total current was measured at 1.1 Amps, the emittance (HWHM) 0.069π cm. mrad. (normalized), and with 550 ma of current within this emittance. For Figure 10 (b) the total current was 185 ma, the emittance 0.025π cm. mrad. (normalized) with 90 ma within this emittance; further, 170 ma were within an emittance of 0.05π cm. mrad. (normalized).

It is interesting to estimate the minimum emittance that would be achievable in the case of ideal extraction optics. In this case the beam divergence and emittance are determined by the ion temperature of the plasma from which the beam is extracted. As described in the previous section the ion temperature of the plasma in the plume was measured at 15 eV, for tantalum with 'typical' arc parameters. This is the temperature in the longitudinal direction, which on the assumption of collisional equilibrium of the plasma within the cathode spots, where presumably the ion temperature is determined, we can take as approximately equal to the transverse ion temperature. The beam angular divergence due to finite transverse ion temperature is given by

$$\theta = \frac{v_\perp}{v_\parallel} = \left(\frac{T_i}{\bar{Q}V_{ext}}\right)^{1/2} \qquad (8)$$

and

$$\varepsilon_{N\,min} = .046\,\pi\,R_o\left(\frac{T_i}{A}\right)^{1/2} \qquad (9)$$

For T_i = 15 eV, V_{ext} = 20 kV, tantalum (A = 181, $\bar{Q} \simeq 3$) and the MEVVA II source for which R_o = 1 cm, one finds that θ = 16 mradians and $\varepsilon_{N\,min}$ = .013π cm. mrad. (normalized). Our measured emittances are greater than this by a factor of several, which is not unreasonable. The beam emittance might be improved by this factor by further optimization of the extraction optics.

(iii) Charge State Distribution

The charge state distribution of the extracted ion beam has been measured using a time-of-flight diagnostic. The measured flight times for the various charge states are well-fitted by the calculated values, usually to within the measurement uncertainty of about 1%. Furthermore, it is usually the case that the spectra are quite clean, with only minimal impurity contamination. Thus we feel confident in our routine use of this diagnostic for the measurement of charge state distribution. We have also measured the charge state spectrum using the more conventional magnetic analysis for a number of particular cases, and the agreement with the time-of-flight results is good. An interesting effect that becomes evident from the magnetic analysis studies is the charge exchange of a fraction of the beam on the background gas, and the consequent birth of a component to the distribution having higher energy per charge state than would be expected on the basis of a normal extraction with no consequent charge exchange. This effect can amount to as much as several tens of percent of the beam in extreme cases; the effect is not evident using the time-of-flight method, which only measures particle velocity. The time-of-flight method provides a good measure of the spectrum immediately following extraction, and is a reliable indicator of the down-stream spectrum provided there is no significant charge exchange of ions along the beam channel.

Figures 11 through 15 show some typical oscillograms of the charge state distributions measured with the time-of-flight diagnostic for several different cathode materials.

Figure 11 shows the data obtained using a lithium cathode ($Z = 3$; 93% $A = 7$ and 7% $A = 6$). In this case the arc current was 175 Amps and

the extraction voltage approximately 17 kV. Oscilloscope sweep speed was 0.5 μsec/cm. The first peak is the 200 nsec wide gate pulse, which in this oscillogram has been added onto the same trace as the detector signal. The main peak, at a delay of about 2.5 μsec, is the $^{7}Li^{+}$ signal. A small $^{6}Li^{+}$ signal can be seen, whose relative amplitude is near the natural isotopic abundance of 7% as expected. A few percent of H^{+} and C^{+} impurities are present also. It's interesting to note that the lithium metal had been stored in oil; this may be the origin of the hydrogen and carbon in this case. Only the singly ionized species is present, for which the ionization potential is 5.3 eV. The second ionization potential is 75 eV, and no Li^{++} is seen in the spectrum. Note also that the arc burning voltage is less than 20 volts, which is consistent with the appearance of the singly ionized species only. (Here and in the following we refer to ionization potential of a given charge state as the energy needed to create the given charge state as the <u>final</u> state of the electron removal process).

Figure 12 shows the spectrum obtained with a titanium cathode, under typical conditions. For titanium, Z = 22 and the isotopic composition is A = 46, 47, 48, 49, 50 with abundances 8, 7, 74, 6, 5%. The spectrum is composed of Ti^{2+} and Ti^{3+}, with only very small fractions of Ti^{+} and Ti^{4+}. This is to be compared to the ionization potentials of 6.1, 13.3, 25.5 and 43.7 eV for the Q = 1,2,3 and 4 ionization states[77].

Figure 13 shows a niobium spectrum, (100% $^{93}_{41}Nb$), for which Nb^{2+}, Nb^{3+} and Nb^{4+} are the dominant components. The ionization potentials are 5.5, 13.9, 26.7, 39.6 and 52.5 eV for Q = 1,2,3,4, and 5[77].

Figure 14 shows a tantalum spectrum (100% $^{181}_{73}Ta$), for which the dominant components are Ta^{3+}, Ta^{4+} and Ta^{5+}, with small amounts of Ta^{2+} and Ta^{6+}. The ionization potentials are 6.8, 14.5, 23.5, 36.3, 49.1 and

92.7 eV for Q = 1,2,3,4,5, and 6 [77].

Finally, Figure 15 shows the spectrum for a uranium beam (100% $^{238}_{92}U$). The dominant species are U^{4+}, U^{5+} and U^{6+}, with small amounts of U^{2+}, U^{3+} and U^{7+}. The ionization potentials are 5.4, 11.6, 18.1, 30.9, 50.0, 68.9 and 90.3 eV for Q = 1,2,3,4,5,6,7[77].

The charge state distribution obtained varies with the arc power input, which is varied experimentally by changing the pulse line charging voltage or by inserting a series resistance in the arc circuit. As is usual for arc discharges of this kind, the arc voltage tends to remain fixed while the arc current changes. The charge state distributions referred to above and shown in Figures 11-15 are for 'typical' arc current, meaning mostly in the range 200-300 Amps. It is observed that the arc voltage is higher for cathodes of high Z material, and in fact is comparable to the ionization potential of the most highly stripped state seen in the spectrum. Thus for example the arc voltage is about 20 volts for aluminum and titanium, but is as high as nearly 100 volts for uranium.

Figure 16 shows a plot of the (interpolated) ionization potential corresponding to the mean charge state of the distribution as a function of the measured arc voltage drop, for tantalum. One can see that there is a correspondence, though not linear.

Figure 17 shows the increase in mean charge state of the spectrum as the arc input power is increased. These data were taken using a tantalum cathode. The variation of $\bar{Q}$ with P is slow. Most of the power variation is through the arc current, and the arc voltage varies only a little, as can be seen from the data of Figure 16.

Time-of-flight spectra obtained in this way provide an indication of the beam charge state distribution at one particular time during the beam extraction pulse. It is of importance to know the variation of charge state distribution as a function of time throughout the beam pulse. Furthermore, although most of our work has been done using an arc pulse length and thus beam extraction pulse length of about 300 μseconds, we also want to be able to run with pulse lengths of several milliseconds, (and for more general application of the source, eventually dc). Figure 18 shows the results of a series of measurements which address these concerns. We constructed an arc pulse line of length 3 msec, the output current pulse shape of which is as seen in the lower trace of Figure 18 (a). Time-of-flight spectra were taken at the times indicated by the markers. The spectra measured at these times are shown in Figure 18 (b) (early times top, later times bottom). We can make the following observations: (a) the beam charge state distribution remains similar throughout the 2.5 msec monitored; (b) the distribution is weighted toward higher charge states earlier in the arc pulse when the arc current is higher; (c) there is a gradual decrease in beam intensity throughout the pulse, as the arc pulse line current droops. Moreover, little jitter in the beam intensity and in the charge state distribution is seen, and shot-to-shot variation is minimal, apart from a smooth decrease which can be ascribed to the falling arc current. (There is a small jitter in flight time because of imperfect extractor supply regulation). We expect that an arc supply designed to hold the arc current more constant would result in an acceptably constant charge state distribution; this remains to be confirmed experimentally.

It is important to realize that the time-of-flight diagnostic provides only an indication of the charge state spectrum, and that there are inherent uncertainties which are difficult to remove. The sensitivity of the detector (an RCA 7265 photomultiplier with the front glass surface removed) as a function of ion species and charge state is unknown. Also, the ion optics of the system may not be charge-state independent, although we routinely vary the potentials of all of the optical elements to check for this effect. Thus one should take these data as indicative of the ion beam charge state distribution, but one should not trust the data completely.

(iv) Beam Noise and Reproducibility

High frequency noise and shot-to-shot variation in beam current are parameters of some importance to users of the beam from any ion source. A detailed study of these features of the MEVVA ion source behavior must wait until we've constructed a good beam analysis and transport system. The beam current fluctuation level and shot-to-shot reproducibility vary considerably depending on the conditions under which we're operating. None-the-less we can make some preliminary observations.

Figure 19 is an oscillogram of an overlay of six shots of the beam current collected by a collector plate. The cathode material was lithium. One can see that in this case the noise and the reproducibility are both fair - $\Delta i/i \leq$ 10-20% or so, both on a microsecond time scale and on a shot-to-shot basis.

In Figure 20 are shown some data on the charge-state-analyzed beam quality. In this experiment we used a cobalt cathode. Figure 20 (a) shows the arc current (lower trace, 200 Amps/cm) and the beam current as measured by a magnetically suppressed Faraday cup (upper trace,100 ma/cm),

sweep speed is 50 μsec/cm. It can be seen that the noise level near the current maximum is approximately 10% or less. Figure 20 (b) shows the time-of-flight charge state spectrum as obtained on five consecutive shots; extraction voltage was 15 kV and sweep speed was 2 μsec/cm. The lower trace is the gating pulse; the three major peaks in the spectrum are Co^{+}, Co^{2+}, and Co^{3+}. (The oscilloscope, a Tektronix Model 468, is a digital storage oscilloscope, and the effect of the digitizing on the trace appearance is evident - note particularly the trace third from the top). One can see that the spectrum is fairly reproducible both in overall magnitude and in shape.

Finally, in Figure 21 is shown the beam current measured by a magnetically-suppressed Faraday cup for the case of a Li^{+} beam at the exit of a dipole bending magnet (analysis magnet). Although the beam optics are not optimum, as previously mentioned, it can be seen that the beam noise is minimal - only a few percent. It is significant to note that in this case we positioned "D-plates" within the analysis magnet to help provide neutralizing electrons by secondary emission from ions striking these metallic boundary plates; without the D-plates the beam noise was greater, ~30% or so.

Based on preliminary indications such as these, we anticipate that the beam quality will be adequate for most applications. Furthermore, there may well be changes in source geometry or operating mode that will enable us to reduce the beam noise level even more.

V. Discussion

A. Ion Beam Extraction

The extraction of ions from a plasma and consequent ion beam formation has been discussed in depth by a number of authors[50-53] and is

well understood theoretically. For a plane-parallel extraction geometry the ion beam current density is given by the Child-Langmuir relation

$$j_i = \frac{4\varepsilon_o}{9}\left(\frac{2eQ}{m_a A}\right)^{1/2}\frac{V^{3/2}}{d^2} \qquad (10)$$

where ε_o is the permittivity of free space, Q and A the ion charge (electronic units) and mass (amu), m_a the mass equal to 1 amu, V the extraction voltage applied across the gap, and d the gap separation. Inserting values this can be written as

$$j_i = 1.72\left(\frac{Q}{A}\right)^{1/2}\frac{V^{3/2}}{d^2} \quad ma/cm^2 \qquad (11)$$

where now V is in kV and d in cm. For a real extractor the plasma boundary (sheath) does not remain plane-parallel, but forms a curved meniscus at the extractor hole. Thus a correction is necessary and the parameter d is replaced by a new effective gap separation, d_{eff}. There seems to be some discussion in the literature as to the correct expression for d_{eff}; we take here the value

$$d_{eff} = d + r_h, \qquad (12)$$

where r_h is the radius of an individual extractor hole. Using now parameters which are typical for our operation - tantalum, A = 181, Q = 3, V = 25kV, d = 0.17 cm, r_h = 0.05 cm - then for an extractor array of 163 holes we obtain finally I = 890 ma. This is in excellent (and perhaps surprising!) agreement with the measured beam current of approximately 1 Amp, and well within the uncertainties in both the experimental determination and the theoretical prediction.

Notwithstanding this self-consistent picture of ion extraction, it is important to note that there are at least two effects that can greatly

increase the extracted beam current over that give by the Child-Langmuir relation. The first effect is due to a non-Maxwellian electron velocity distribution and consequent reduction of the ion space charge within the accelerating gap[78,79]. In a beam-plasma type ion source, where the electron velocity distribution can be far from Maxwellian, an observed order-of-magnitude increase in extracted ion current has been ascribed to this effect. The second effect is due to the ion flow, or streaming, velocity and the consequent increased flux of ions across the Langmuir sheath[80]. For a stationary plasma the ion flux across a sheath is given by the Bohm formula[81]

$$j_B = 0.4\ ne \left(\frac{2kT_e}{m_i}\right)^{\frac{1}{2}}, \qquad (13)$$

where the ion velocity through the sheath is proportional to the ion acoustic velocity. If the ions enter the sheath with an additional velocity, their drift velocity v_D, on top of the random thermal speed, then the ion flux across the sheath is increased above the Bohm value by the factor v_D/c_s, where c_s is the ion acoustic velocity. The important point here is that the correct comparison is the ion drift energy to the electron temperature and not the ion drift energy to the extraction potential. The extraction potential determines the ion beam energy, but the ion beam density is determined (in part) by the plasma electron temperature, via the sheath.

B. Charge State Distribution

It is interesting to consider the charge state distribution in a little more detail. The spectrum shown in Figure 14, a tantalum spectrum, is typical of what is observed. We show below that a charge state spectrum of this shape can be explained by a conventional picture of stepwise ionization by electron impact, and that the plasma parameters

implied are in order-of-magnitude agreement with those expected for a vacuum arc.

Ions are created by ionization from the neutral state by electron impact. The plasma ions may be stripped by a number of different processes, but the most important process is stepwise ionization by successive electron impact[82]. As one intuitively expects, the maximum charge state that can be obtained is determined by (i) the electron temperature T_e, and (ii) the product $n_e \tau_i$ of electron density n_e and ion confinement time τ_i. Thus the plasma electrons must be sufficiently energetic to remove the bound electrons by collisions, and the plasma electron density and ion residence time within the plasma must be sufficiently great to allow the stripping to proceed. Calculations of the parameters necessary to achieve different charge states for a variety of elements have been carried out by a number of authors[83-85], and involve evaluating expressions of the type

$$n_e \tau_i(Q) = \sum_{k=o}^{Q-1} \frac{1}{\langle \sigma_{k,k+1} v_e \rangle} \qquad (14)$$

where τ_i (Q) is the time which must elapse to produce ions of charge state Q, $\sigma_{k,k+1}$ is the cross section for ionization from charge state k to charge state k+1 by impact with electrons of velocity v_e, and the average $\langle \sigma v \rangle$ is taken over the distribution of electron velocities. The cross sections can be taken as given by the semi-empirical formula of Lotz[86]. It is often more appropriate to consider the parameter $j\tau$ rather than $n\tau$, where j is the electron current density; trivially,

$$j\tau = n\tau e v_e .$$

In this discussion we ignore the difference between the electron energy E_e for the case of a directed beam of electrons and the electron temperature

T_e for the case of a Maxwellian plasma, and note that the results are insensitive to the electron distribution[84].

Results of a calculation of $j\tau$ (E_e) for tantalum are shown in Figure 22. For a given charge state, the required $j\tau$ becomes finite at an energy equal to the ionization potential for that charge state and has a broad minimum at an energy several times the ionization potential, corresponding to the maximum of the ionization cross section that occurs at several times the ionization potential. Data such as this thus allow a prediction of the plasma parameters required to produce a particular ion in a particular charge state.

We have carried out a similar calculation[87] choosing the input parameters so as to provide a best fit to the experimental data for tantalum as in Figure 14. The results of this calculation are shown in Figure 23. Here, the evolution of the various charge states is shown as a function of $j\tau$. In this calculation the electron energy E_e = 94.5 eV, and a 7% background of neutral tantalum is continually introduced, thus allowing the low charge state fractions to maintain a non-zero asymptote rather than burning out. In this plot the changing charge state distribution of the stripped tantalum plasma is given, and the distribution at $j\tau = 4 \times 10^{16}$ electrons/cm^2 sec is shown in Table I together with the measured spectrum of Figure 14. The agreement is excellent. Similarly and as expected, these parameters locate us in the correct region of Figure 22. To some extent the agreement may be fortuitous, since the variation in time-of-flight detector sensitivity with charge state is unknown; thus we should not ascribe too much quantitative significance to the precise values of the parameters of the fit.

These implied values of $j\tau$ (or $n\tau$) and E_e can be compared with estimated plasma parameters. If we assume that the ionization process is limited to the cathode spot plasma, then the above value of $j\tau$ will be satisfied by a current density of several megamperes/cm^2, a spot size of several microns, and an average streaming energy of a tantalum ion through the cathode spot plasma region of about 10 eV. These values are certainly well within the uncertainty of our knowledge of the cathode spot plasma parameters. One can also make a comparison with the parameters of the arc plasma filling the space between cathode and anode. In this case a current density of several kilo-amperes/cm^2 and an ion drift energy of only 1 eV or so are needed to meet the required $j\tau$. These parameters seem improbable, and thus the fit to this scenario - ionization within the main arc region - is not good. Providing further corroboration of this interpretation is the experimental observation that the measured charge state distribution does not change as the cathode - anode separation, and so also the ion residence time within the arc, is changed over a factor of two or more.

We conclude that the measured ion charge state distribution can be explained by stepwise ionization within the cathode spot plasma. The implied current density - ion confinement time product, $j\tau$, is in good agreement with what one might expect at the cathode spots, but the implied plasma electron temperature is higher than expected. Although ionization in the main arc region between cathode and anode cannot be ruled out, stripping seems to probably be a function of the cathode spots and not of the main arc.

VI. Conclusion

We have described an ion source whose novel feature lies in the high current metal ion beams that can be produced. An arc discharge is established in vacuum between metal electrodes and the ion beam is extracted from the intense plume of metal vapor plasma so produced. We have investigated some of the basic performance characteristics of the source and the results of these measurements have been described.

A lot of research remains to be done to understand the source more fully, and development to optimize its embodiment and performance. It is probable that the version we've described here can be improved upon greatly.

The closely related concern of the transport of high current, high mass ion beams of the kind produced here is a field of investigation that must be addressed also. Although some applications do not require magnetic charge state analysis nor transport of the beam over long distances, many applications do. Full exploitation of the high current beams such as described here will need a good understanding of high current beam transport in neutralization-unfriendly environments.

We expect that the source will undergo considerable evolution and that it will find application in a wide variety of fields.

References

1. 1984 Annual Report, Accelerator and Fusion Research Division, Lawrence Berkeley Laboratory, LBL-19100, (1985).
2. W. B. Kunkel in "Fusion", E. Teller, ed., Academic Press, New York (1981).
3. S. Humphries, Jr., Nuclear Fusion 20, 1549 (1980).
4. S. Humphries, Jr., R. N. Sudan and L. Wiley, J. Appl. Phys. 47, 2382 (1976).
5. S. Humphries, Jr., C. Eichenberger and R. N. Sudan, J. Appl. Phys. 48, 2738 (1977).
6. J. M. Neri, D. A. Hammer, G. Ginet and R. N. Sudan, Appl. Phys. Lett. 37, 101 (1980).
7. J. M. Neri and D. A. Hammer, IEEE Trans. Nucl. Sci. NS-28, 3378 (1981).
8. Proceedings of the Fifth International Conference on Ion Implantation Equipment and Techniques, Smugglers' Notch, VT, July 1984, Nucl. Instrum. and Methods B6, (1985).
9. S. T. Picraux, in "Physics Today", Nov. 1984.
10. P. Sioshansi, Thin Solid Films 118, 61 (1984).
11. "Ion Implantation Metallurgy", C. M. Preece and J. K. Hirvonen, ed., The Metallurgical Society of AIM, Warrendale, PA, 1980.
12. L. Valyi, "Atom and Ion Sources", John Wiley and Sons, New York, 1977.
13. J. Ishikawa and T. Takagi, Japanese J. Appl. Phys. 22, 534 (1983).
14. J. Ishikawa, Y. Takeiri and T. Takagi, Rev. Sci. Instrum. 55, 449 (1984).
15. A. Rockett, S. A. Barnett and J. E. Greene, J. Vac. Sci. Technol. B2, 306 (1984).
16. A. Warwick, in Heavy Ion Fusion End of the Year Report, Dec. 1984, Lawrence Berkeley Laboratory, LBL-18840.
17. R. K. Feeney, W. E. Sayle, II, and J. W. Hooper, Rev. Sci. Instrum. 47, 964 (1976).

18. I. C. Lyon and B. Peart, J. Phys. E: Scientific Instrum. 17, 920 (1984).

19. B. Gavin, S. Abbott, R. MacGill, R. Sorensen, J. Staples and R. Thatcher, IEEE Trans. Nucl. Sci. NS-28, 2684 (1981).

20. Y. Saito, Y. Mitsuoka and S. Suganomata, Rev. Sci. Instrum. 55, 1760 (1984).

21. R. W. Sorensen and H. E. Mendenhall, Trans. AIEE, Pt. III, 45, 1102 (1926).

22. J. D. Cobine, Elect. Eng. 81, 13 (1962).

23. J. M. Lafferty, ed., "Vacuum Arcs - Theory and Application", John Wiley and Sons, New York, 1980.

24. B. Edlen, Physica 13, 544 (1947).

25. W. A. Cilliers, R. V. Datla and H. R. Griem, Phys. Rev. A12, 1408 (1975).

26. A. A. Plyutto, Sov. Phys. JETP 12 (6), 1106 (1961).

27. S. Takagi, S. Ohtani, K. Kadota and J. Fujita, Nucl. Instrum. and Methods 213, 539 (1983).

28. A. A. Plyutto, V. N. Ryzhhov and A. T. Kapin, Sov. Phys. JETP 20 (2), 328 (1965).

29. W. D. Davis and H. C. Miller, J. Appl. Phys. 40, 2212 (1969).

30. C. W. Kimblin, Proc. IEEE 59, 546 (1971).

31. C. W. Kimblin, J. Appl. Phys. 44, 3074 (1973).

32. J. E. Daalder and P. G. E. Wielders, Proc. 12th Int. Conf. on Phenomena in Ionized Gases, Eindhoven (Amsterdam: North-Holland), Pt. 1, p. 232.

33. I. Jorde, J. Kulsetas and W. G. J. Rondeel, Proc. 12th Int. Conf. on Phenomena in Ionized Gases, Eindhoven (Amsterdam: North-Holland), Pt. 1, p. 240.

34. J. W. Robinson and M. Ham, IEEE Trans. on Plasma Science, PS-3, 222 (1975).

35. J. E. Daalder, J. Phys. D: Appl. Phys. 8, 1647 (1975).

36. J. L. Hirshfield, IEEE Trans. on Nucl. Science, NS-23, 1006 (1976).

37. J. E. Daalder, J. Phys. D: Appl. Phys. 9, 2379 (1976).

38. "Electromagnetic Separation of Isotopes in Commercial Quantites", R. K. Wakerling and A. Guthrie, eds, National Nuclear Energy Series, USAEC, 1951; page 324.

39. E. I. Revutskii, G. M. Skoromnyi, Yu. F. Kulygin and I. I. Goncharenko, Proc. Sov. Conf. on Charged-Particle Accelerators, Moscow, 9-16 October 1968, A. A. Vasilev, ed., (U.S.A.E.C., pub.) vol. 1, p. 447.

40. S. Coffey, G. Cooper, S. Humphries, Jr., M. Savage and D. Woodall, Bull. Am. Phys. Soc. 29, 1314 (1984).

41. C. Burkhart, S. Coffey, G. Cooper, S. Humphries, Jr., L. K. Len, A. D. Logan, M. Savage and D. M. Woodall, Nucl. Instrum. and Methods B10/11, 792 (1985).

42. R. J. Adler and S. T. Picraux, Nucl. Instrum. and Methods B6, 123 91985).

43. A. S. Gilmour, Jr., and D. L. Lockwood, Proc. IEEE 60, 977 (1972).

44. I. G. Brown, J. E. Galvin and R. A. MacGill, Appl. Phys. Lett. 47, 358 (1985).

45. I. G. Brown, paper presented at the 1985 Particle Accelerator Conference, Vancouver, B.C., May 1985; proceedings to be published in IEEE Trans. Nucl. Sci., Oct. 1985.

46. E. Hantzsche, Proc. 13th Int. Conf. on Phenomena in Ionized Gases (Berlin), vol. 3, p. 121 (1977).

47. IEEE Trans. on Plasma Science, special issue on vacuum discharge plasmas, IEEE PS-11, Sept. 1983.

48. J. A. Rich, L. E. Prescott and J. D. Cobine, J. Appl. Phys. 42, 587 (1971).

49. C. W. Kimblin, Proc. 12th Int. Conf. on Phenomena in Ionized Gases, Eindhoven (Amsterdam: North-Holland), Pt. 1, p. 243.

50. I. Chavet, Proc. Int. Conf. Electromagnetic Isotope Separators, Marburg (BMBW-FBK 70-28), 303, (1970).

51. J. R. Coupland, T. S. Green, D. P. Hammond and A. C. Riviere, Rev. Sci. Instrum. 44, 1258 (1973).

52. T. S. Green, Reports on Progress in Physics 37, 1257 (1974).

53. T. S. Green, IEEE Trans. Nucl. Sci. NS-23, 918 (1976).

54. "An Introduction to Discharge and Plasma Physics", S. C. Haydon, ed., University of New England, Armidale, Austalia, 1964.

55. J. M. Lafferty, Proc. IEEE 54, 23 (1966).

56. N. Vidyardhi and R. S. N. Rau, J. Phys. E: Sci. Instrum. 6, 33 (1973).

57. S. Kamakshaiah and R. S. N. Rau, J. Phys. D: Appl. Phys. 8, 1426 (1975).

58. S. Kamakshaiah and R. S. N. Rau, IEEE Trans. Plasma Science, PS-5, 164 (1977).

59. R. L. Boxman, IEEE Trans. Electron Devices, ED-24, 122 (1977).

60. S. Kamakshaiah and R. S. N. Rau, J. Phys. D: Appl. Phys. 10, 1017 (1977).

61. B. Lehnert, Plasma Physics 9, 301 (1967).

62. J. D. Jukes, Reports on Progress in Physics, 31, 333 (1968).

63. W. M. Manheimer and C. Lashmore-Davies, "MHD Instabilities in Simple Plasma Configurations", Naval Research Laboratory, Wash. D.C., 1984.

64. Beckman and Whitley, Inc., Model 501.

65. V. Joshi, Institute for Plasmaphysics, Garching, Munich, Report IPP 2/83, August 1969.

66. J. Reece Roth and M. Clark, Plasma Physics 11, 131 (1969).

67. J. M. Buzzi, H. J. Doucet and D. Gresillon, Phys. Fluids 13, 3041 (1970).

68. S. A. Andersen, V. O. Jensen, P. Michelsen and P. Nielsen, Phys. Fluids 14, 728 (1971).

69. I. G. Brown, Plasma Physics 18, 205 (1976).

70. F. F. Chen, in "Plasma Diagnostic Techniques", R. H. Huddlestone and S. L. Leonard, ed, Academic Press, New York, 1965.

71. J. W. Staples, H. D. Lancaster and R. B. Yourd, IEEE Trans. Nucl. Sci. NS-28, 3479 (1981).

72. J. R. Alonso, R. T. Avery, T. Elioff, R. J. Force, H. A. Grunder, H. D. Lancaster, E. J. Lofgren, J. R. Meneghetti, F. B. Selph, R. R. Stevenson, and R. B. Yourd, Science 217, 1135 (1982).

73. J. R. Alonso, IEEE Trans. Nucl. Sci. NS-30, 1988 (1983).

74. H. Gould, D. Greiner, P. Lindstrom. T. J. M. Symons, and H. Crawford, Phys. Rev. Letters 52, 180 (1984).

75. J. E. Galvin and I. G. Brown, Rev. Sci. Instrum. 55, 1866 (1984).

76. J. E. Galvin and I. G. Brown, Lawrence Berkeley Laboratory Report LBL-18815; accepted for publication in Rev. Sci. Instrum.

77. T. A. Carlson, C. W. Nestor, Jr., N. Wasserman and J. D. McDowell, Atomic Data 2, 63 (1970).

78. R. A. Demirkhanov, Yu. V. Kursanov and L. P. Skripal', Sov. Phys. - Tech. Phys. 15, 1047 (1971).

79. M. G. Rosing and J. R. Conrad, J. Appl. Phys. 57, 816 (1985).

80. M. Dembinski and P. K. John, J. Appl. Phys. 50, 6113 (1979).

81. D. Bohm, E. H. S. Burhop and H. S. W. Massey, in the "The Characteristics of Electrical Discharges in Gases", ed. A. Guthrie and R. K. Wakerling, McGraw Hill, New York, 1949.

82. B. L. Schram, Physica 32, 197 (1966).

83. H. Winter and B. H. Wolf, in "Proceedings of the Second Symposium on Ion Sources and Formation of Ion Beams", Berkeley, California, October 1974; Lawrence Berkeley Laboratory Report LBL-3399, paper V-1-1.

84. H. Winter, in "Experimental Methods in Heavy Ion Physics", Lecture Notes in Physics Series, ed. K. Bethge, Springer-Verlag, Berlin, 1978, page 14.

85. SFEC Group, Report SFEC T 10 - Cryebis II, Laboratoire National Saturne, Saclay, France, 1981.

86. W. Lotz, Zeits. fur Physik 216, 241 (1968).

87. We are indebted to Dr. B. Feinberg, who wrote the computer program.

Figure Captions

Fig. 1 Outline of the MEVVA ion source. The embodiment indicated is that of MEVVA II.

Fig. 2 Photograph of the partially disassembled MEVVA II source.

Fig. 3 Photograph of MEVVA III.

Fig. 4 Schematic of the source electrical configuration.

Fig. 5 Oscillogram of arc voltage and current. Cobalt cathode.

Fig. 6 Sequence of framing camera exposures showing evolution of the cathode spots throughout the arc history. MEVVA I; exposure time = 8 μseconds.

Fig. 7 Photograph of the plasma plume, streaming through the 1 cm diameter anode hole (left) and ducted along the magnetic field toward the extractor grid (right). Uranium plasma in MEVVA I.

Fig. 8 Ion energy analysis of the expanding plasma plume. The current to the collector plate is measured as a function of the collector voltage; first grid grounded, second grid biased to repel electrons (-225V). The ion temperature is measured to be 15 eV.

Fig. 9 Beam radius, R, (HWHM) vs axial distance, z from source. MEVVA II with tantalum cathode; extraction voltage 15 kV.

Fig. 10 Measured beam profile and fitted Gaussian. Axial distance from source to detector is 100 cm and the radial separation between individual current collectors is 1.7 cm.

(a) High current beam; tantalum, 25 kV.

(b) Collimated beam; tantalum, 20 kV.

Fig. 11 Time-of-flight charge state distribution obtained using a lithium cathode. Sweep speed 0.5 μsec/cm; extraction voltage approx. 17 kV.

Fig. 12 Time-of-flight charge state distribution obtained using a titanium cathode. Sweep speed 1 μsec/cm; extraction voltage approx. 11.5 kV.

Fig. 13 Time-of-flight charge state distribution obtained using a niobium cathode. Sweep speed 2 μsec/cm; extraction voltage approx. 11.5 kV.

Fig. 14 Time-of-flight charge state spectrum obtained using a tantalum cathode. Sweep speed 2 μsec/cm; extraction voltage approx. 5 kV.

Fig. 15 Time-of-flight charge state spectrum obtained using a uranium cathode. Sweep speed 2 μsec/cm; extraction voltage approx. 6 kV.

Fig. 16 Interpolated ionization potential of the average of the charge state spectrum vs. the measured arc voltage drop. Tantalum cathode.

Fig. 17 Mean charge state of the time-of-flight charge state spectrum vs. arc input power. Tantalum cathode.

Fig. 18 (a) Long pulse arc current and time-of-flight timing markers.
Sweep speed 1 msec/cm.

(b) Time-of-flight CSD for the times indicated in (a).
Early times top, late times bottom. Tantalum cathode.

Fig. 19 Oscillogram of the beam current to a Faraday cup. Lithium cathode. This is an overlay of 6 consecutive shots, showing the beam noise and reproducibility.

Fig. 20 Reproducibility in time-of-flight charge state spectrum. Colbalt cathode.

(a) Upper trace: beam current, 100 ma/cm
Lower trace: arc current, 200 Amps/cm
Sweep speed 50 μsec/cm.

(b) Upper five traces: time-of-flight spectrum, 5 consecutive shots
Lower trace: gate pulse
Sweep speed 2 μsec/cm.

Fig. 21 Beam current measured by a magnetically-suppressed Faraday Cup at the exit of the dipole charge-state-analysis magnet. Li^+.

Fig. 22 Plasma parameters necessary to strip tantalum to a given charge state.

Fig. 23 Evolution of the charge state distribution with time. Tantalum.

Table I. Theoretical vs. experimental charge state distribution for tantalum. Theoretical: from Figure 23 at $j_\tau = 4 \times 10^{16}$ electrons/cm^2 sec. Experimental: from Figures 14.

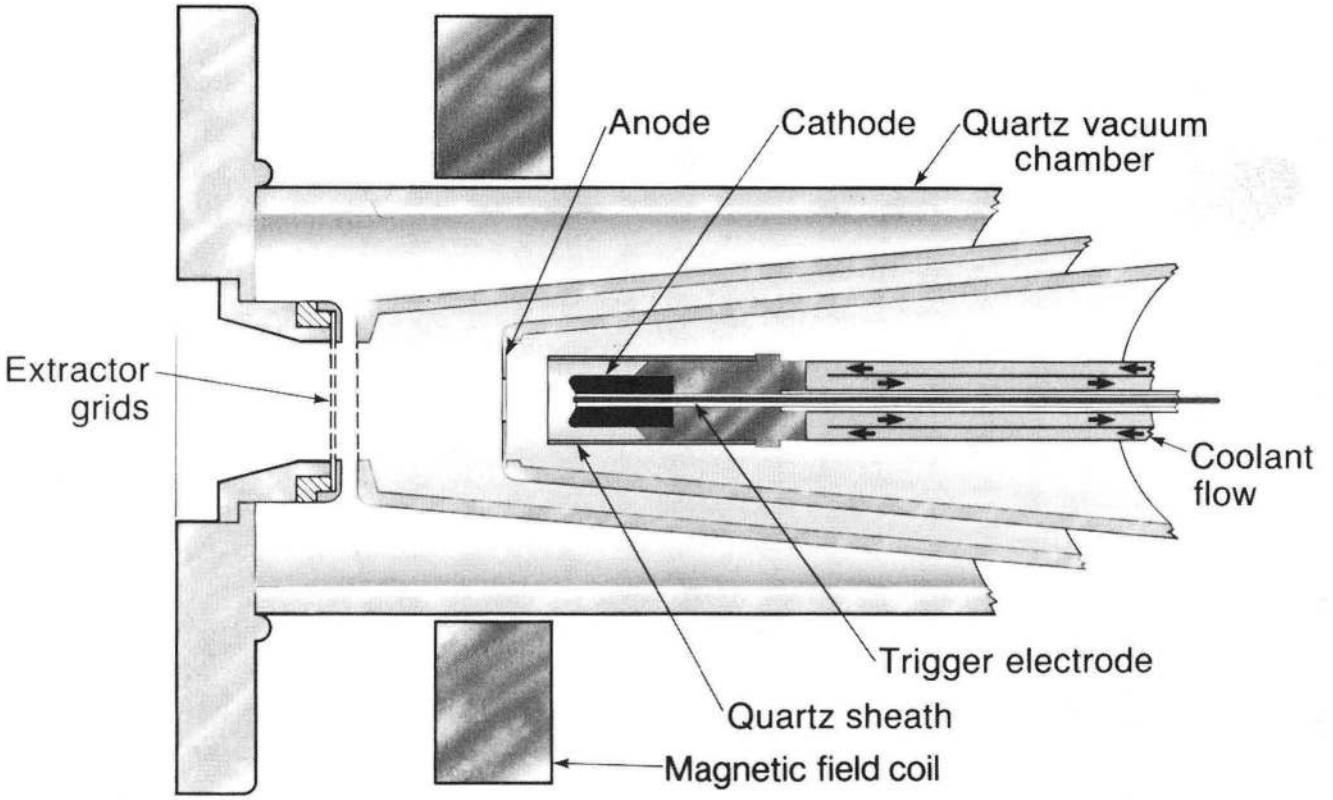

Fig. 1

CBB 854-3258

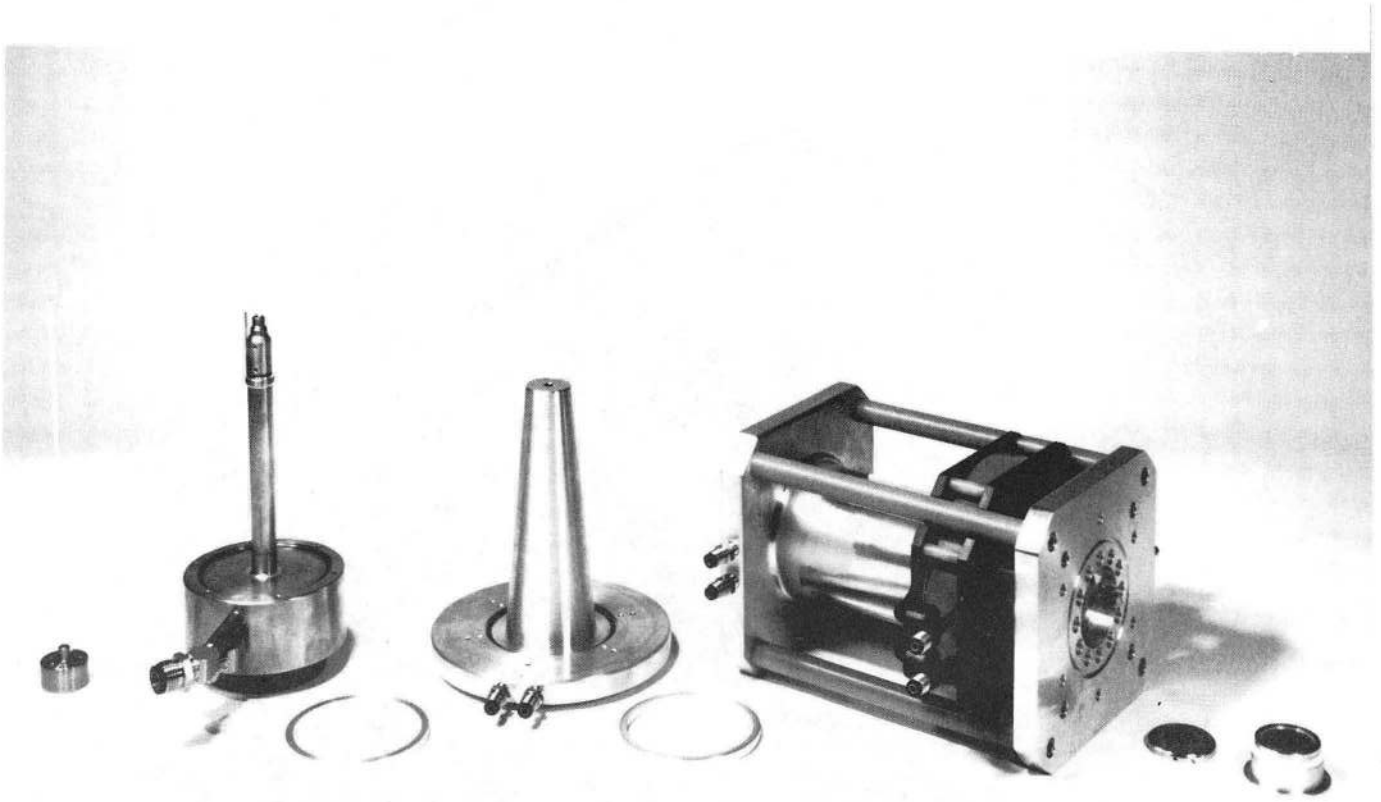

Fig. 2

CBB 844-2814

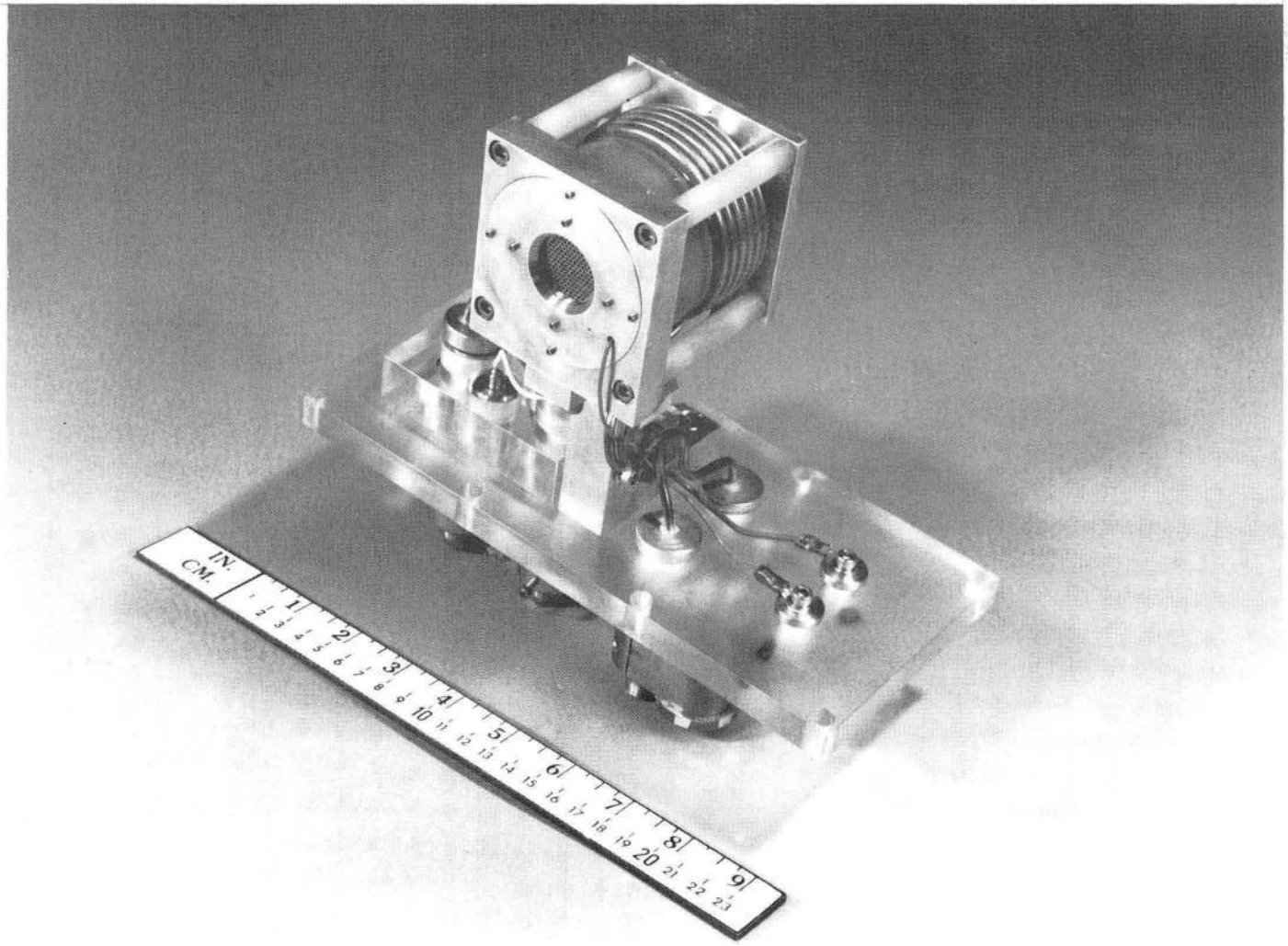

Fig. 3

CBB 840-7619

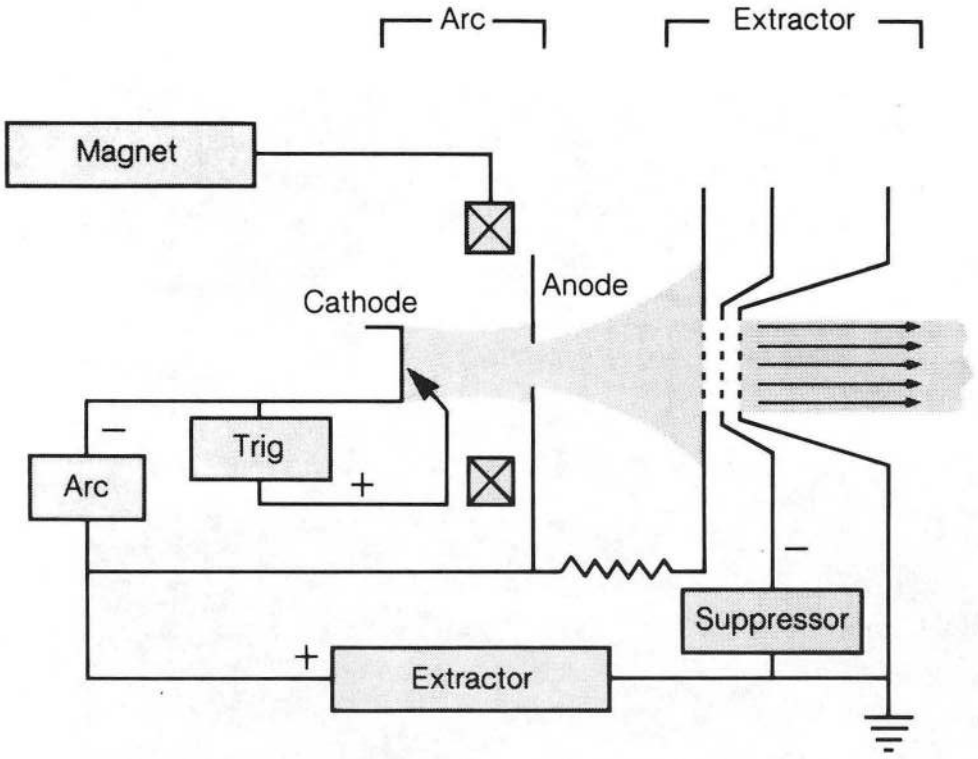

Fig. 4

XBL 858-9895 A

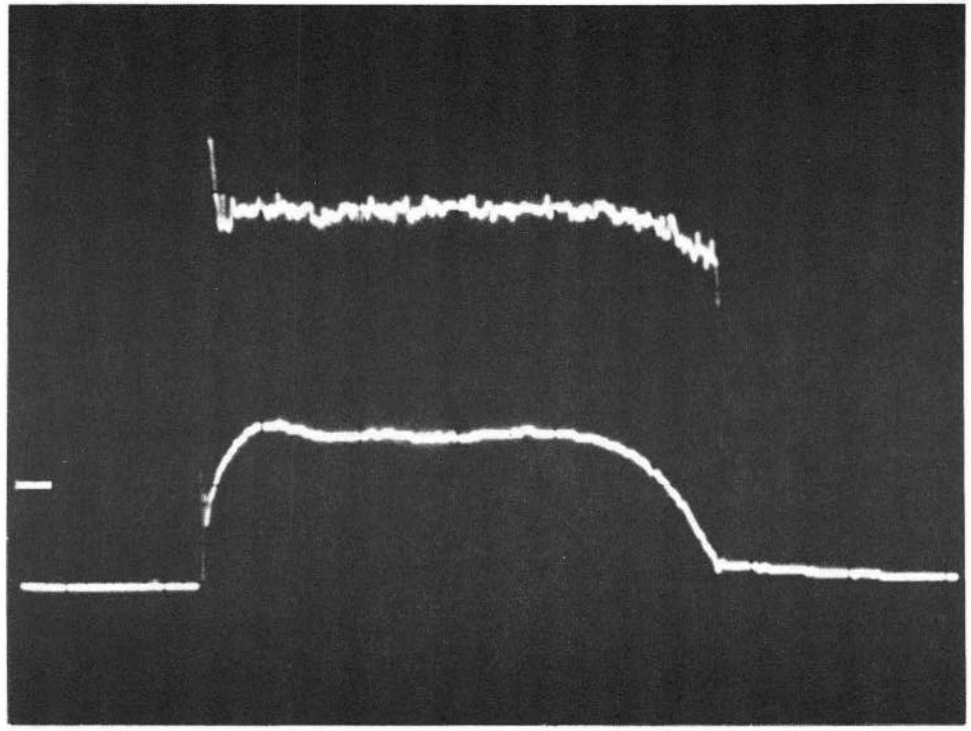

Fig. 5

XBB 858-6533

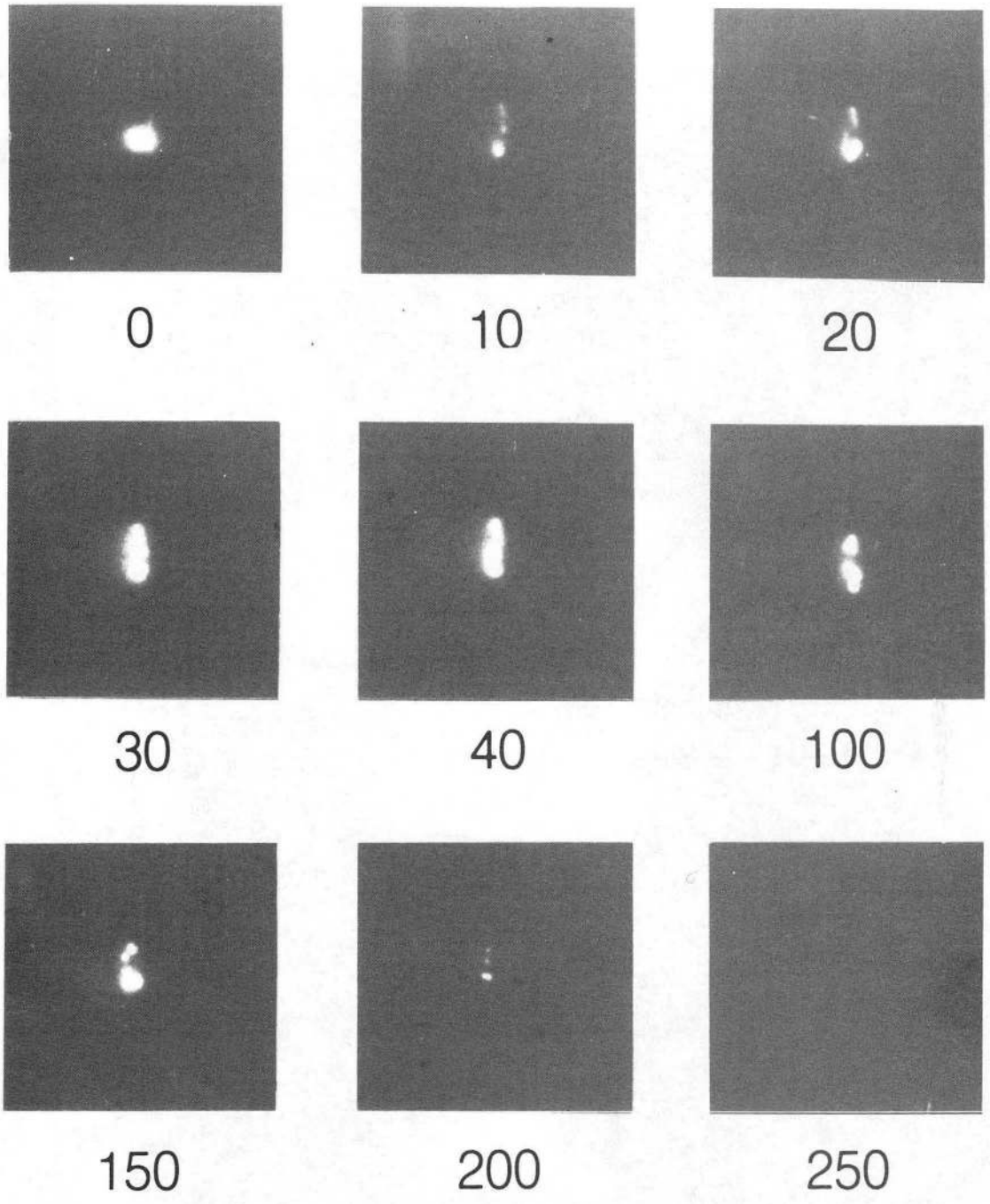

Fig. 6

XBB 858-6324A

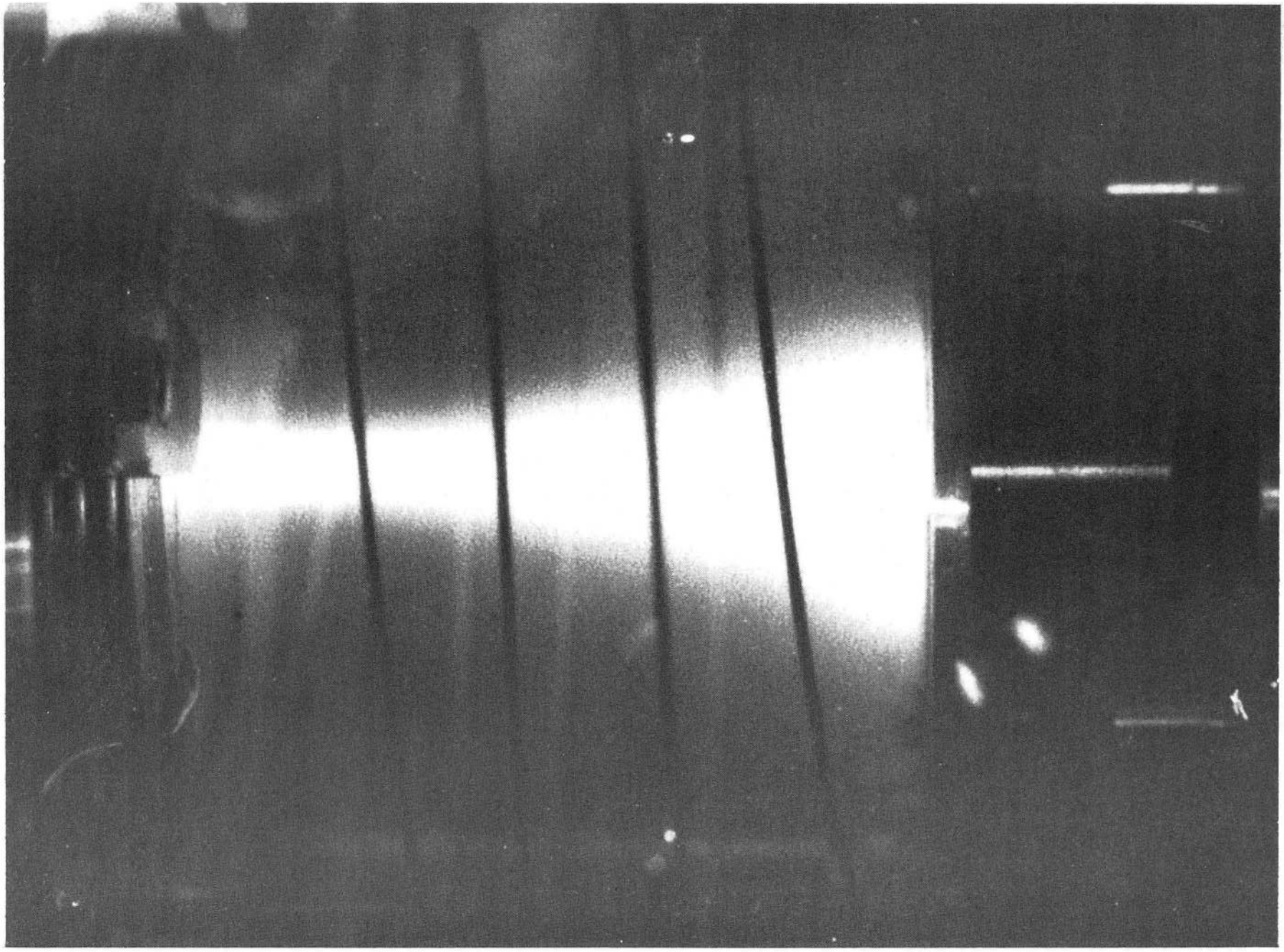

Fig. 7

CBB 830-11075

ION ENERGY ANALYSIS

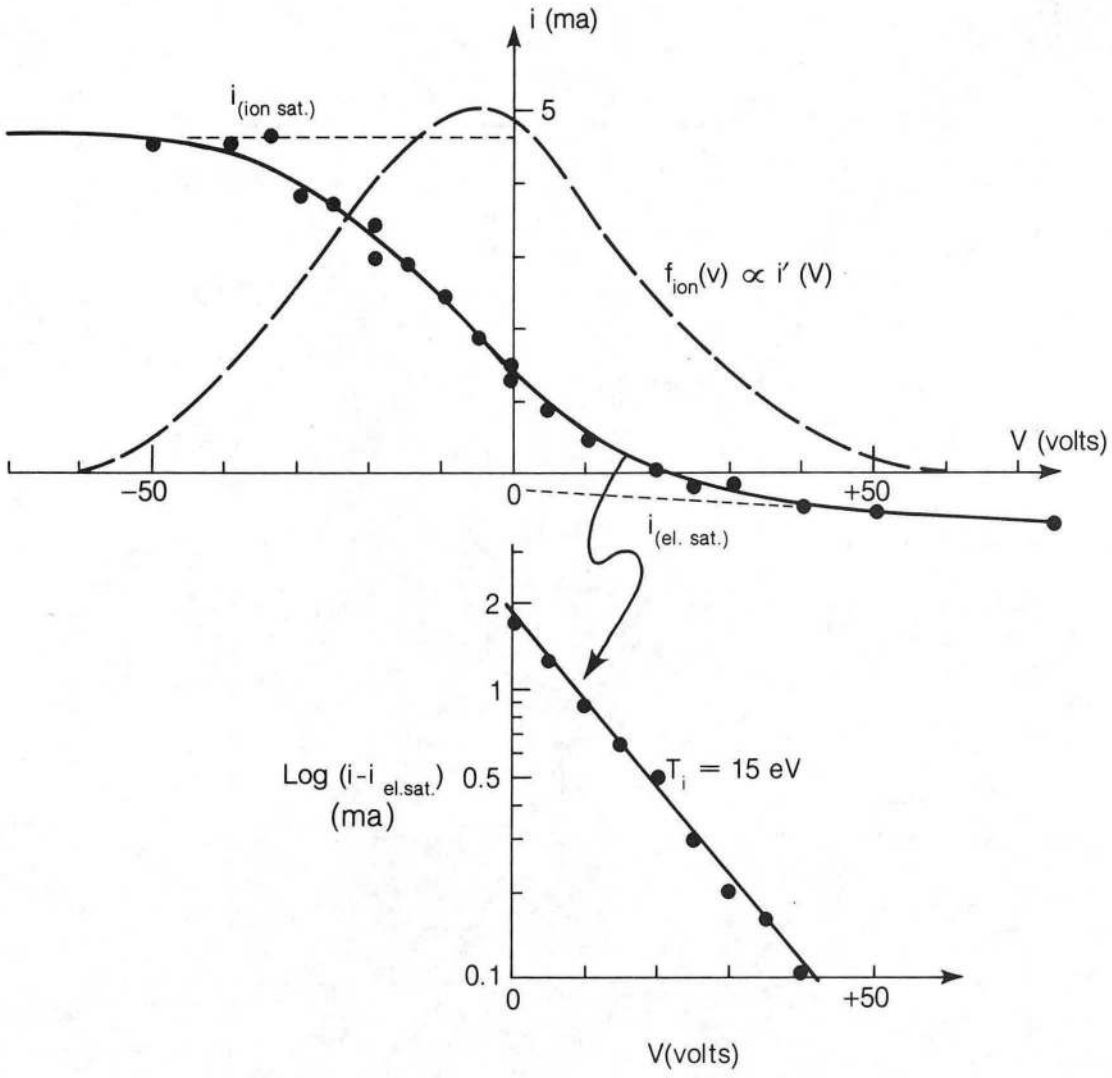

XBL 838-529A

Fig. 8

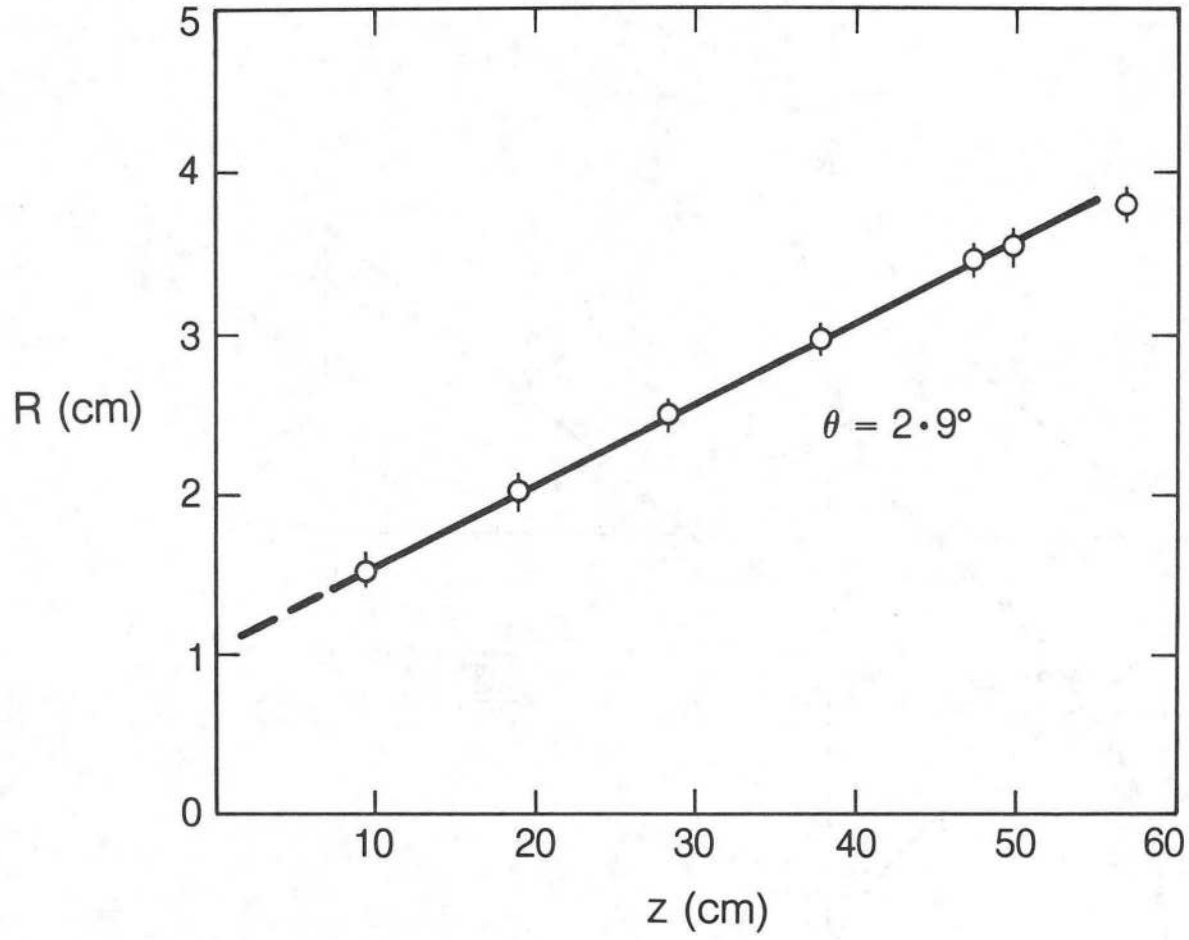

Fig. 9

XBL 854-9939

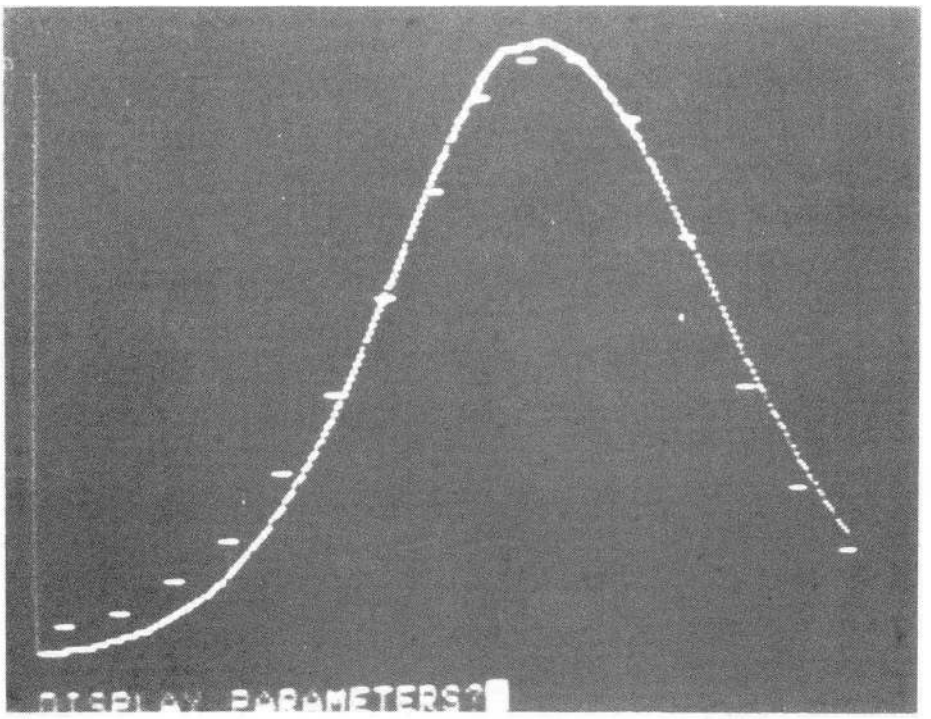

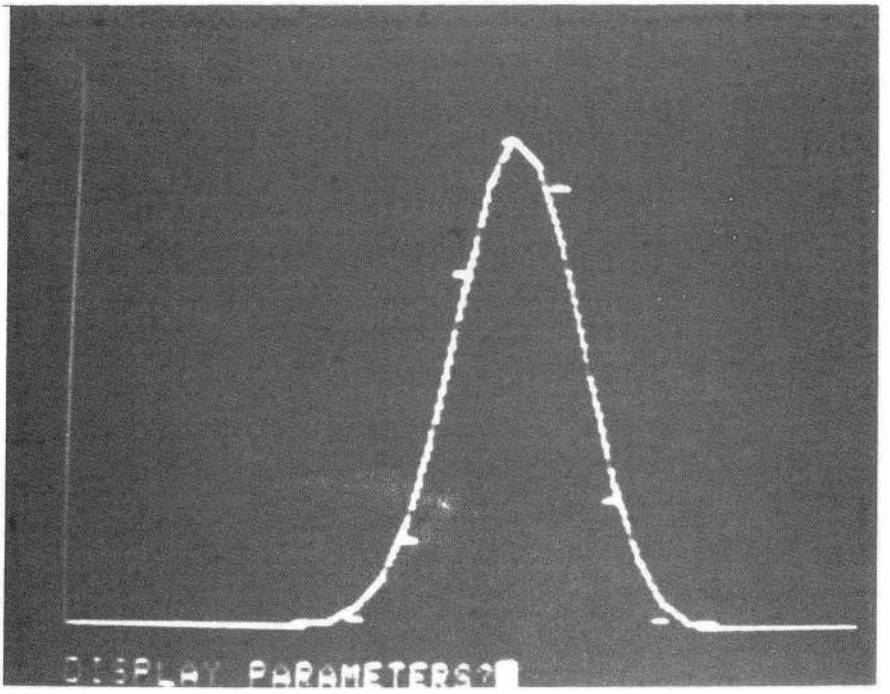

Fig. 10 XBB 840-9238B

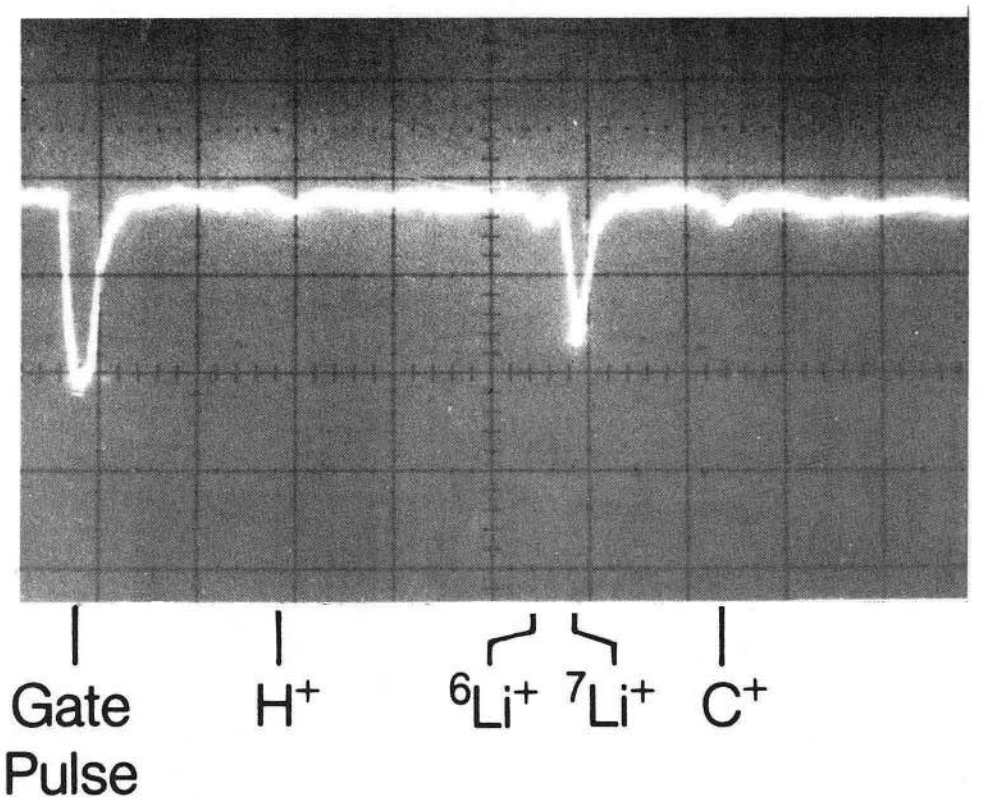

Fig. 11

XBB 854-3253

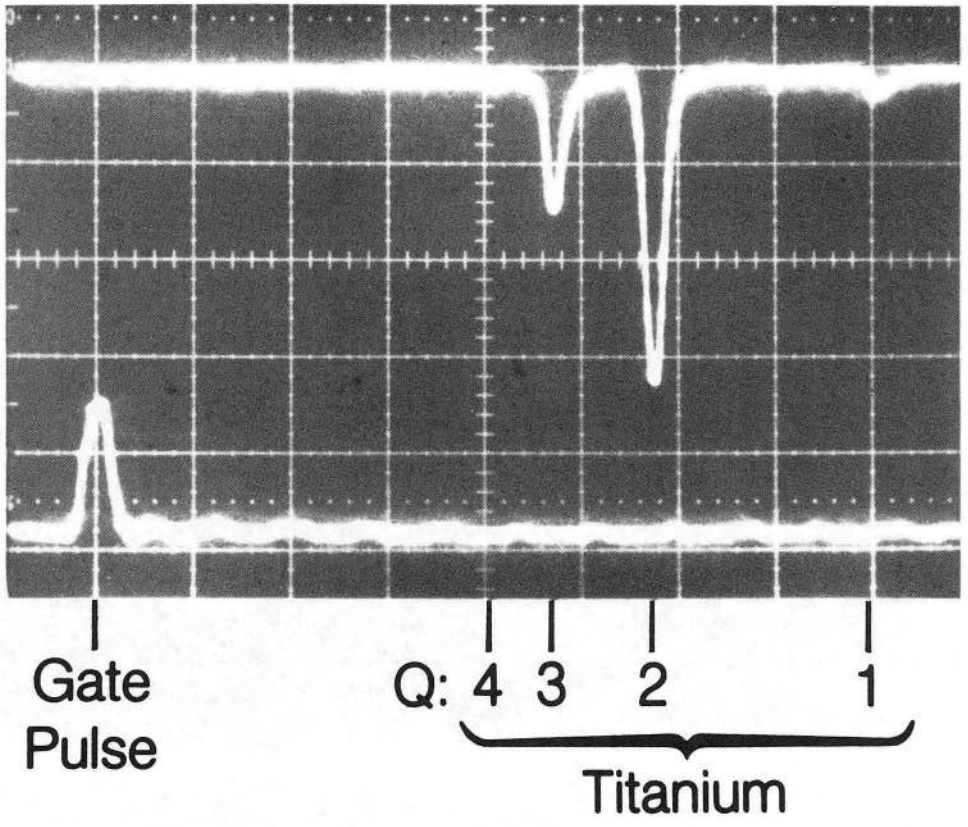

Fig. 12

XBB 854-3256

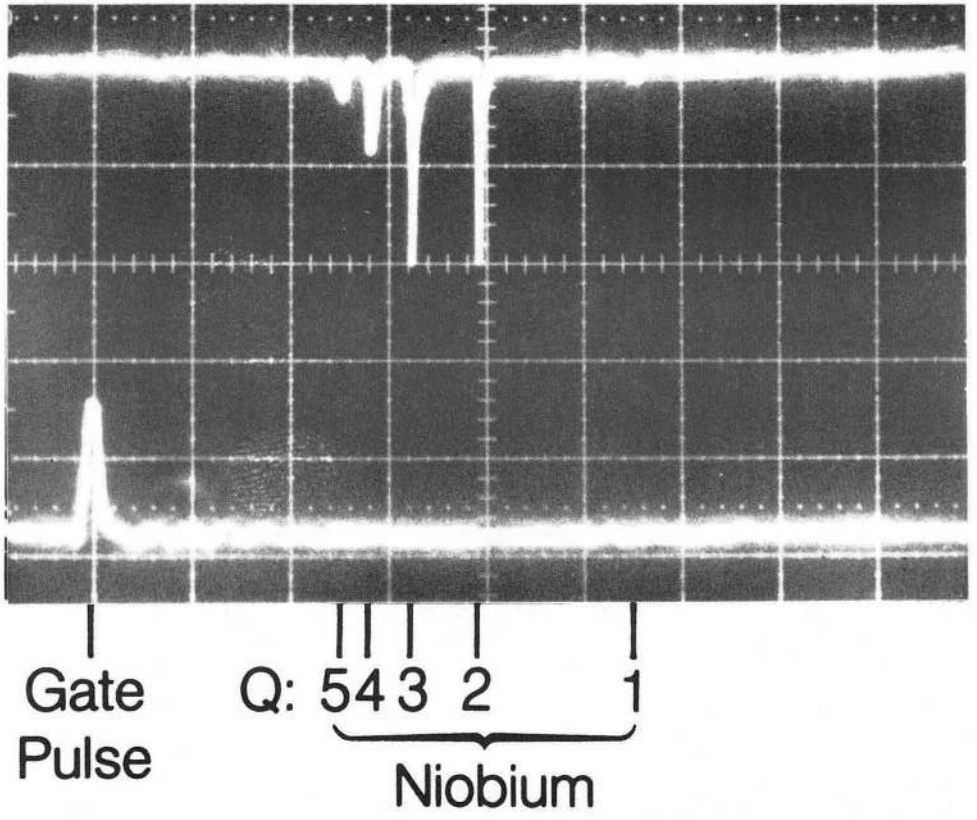

Fig. 13

XBB 854-3255

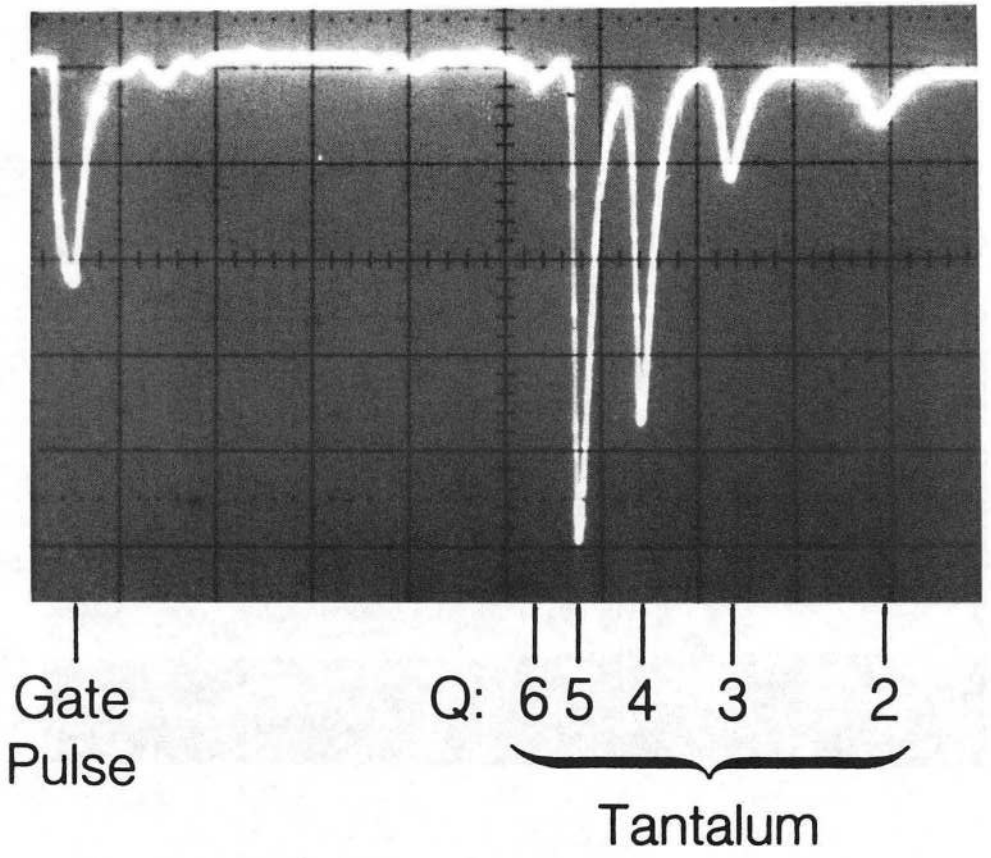

Fig. 14

XBB 858-6183

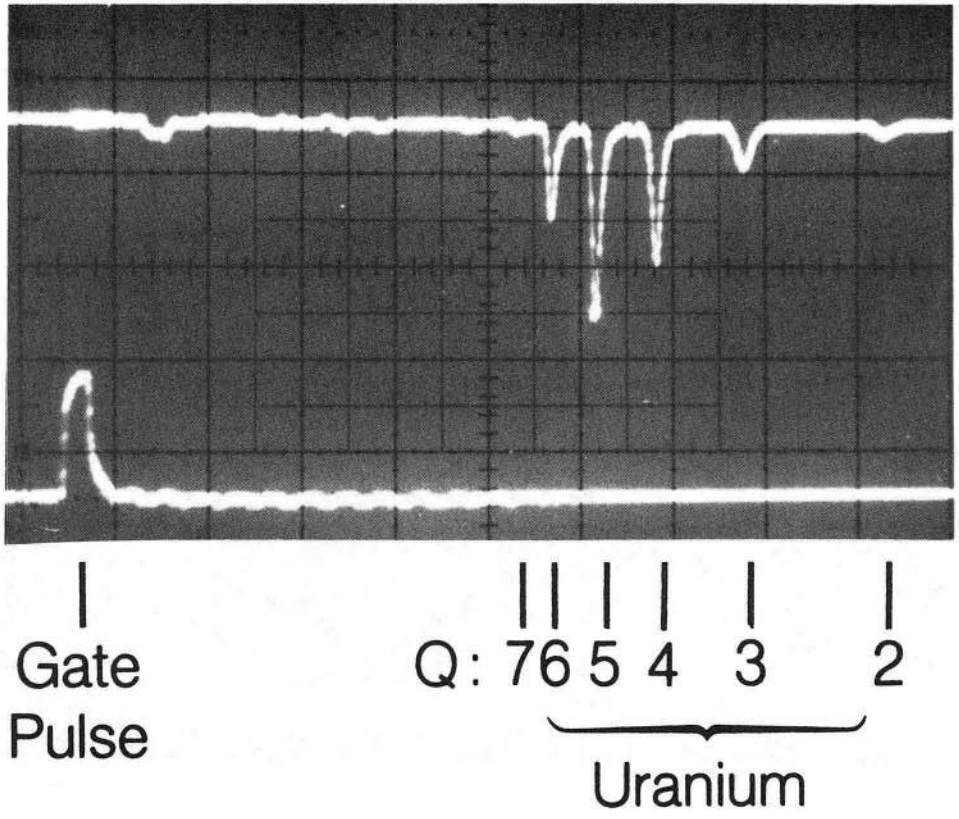

Fig. 15

XBB 854-3522

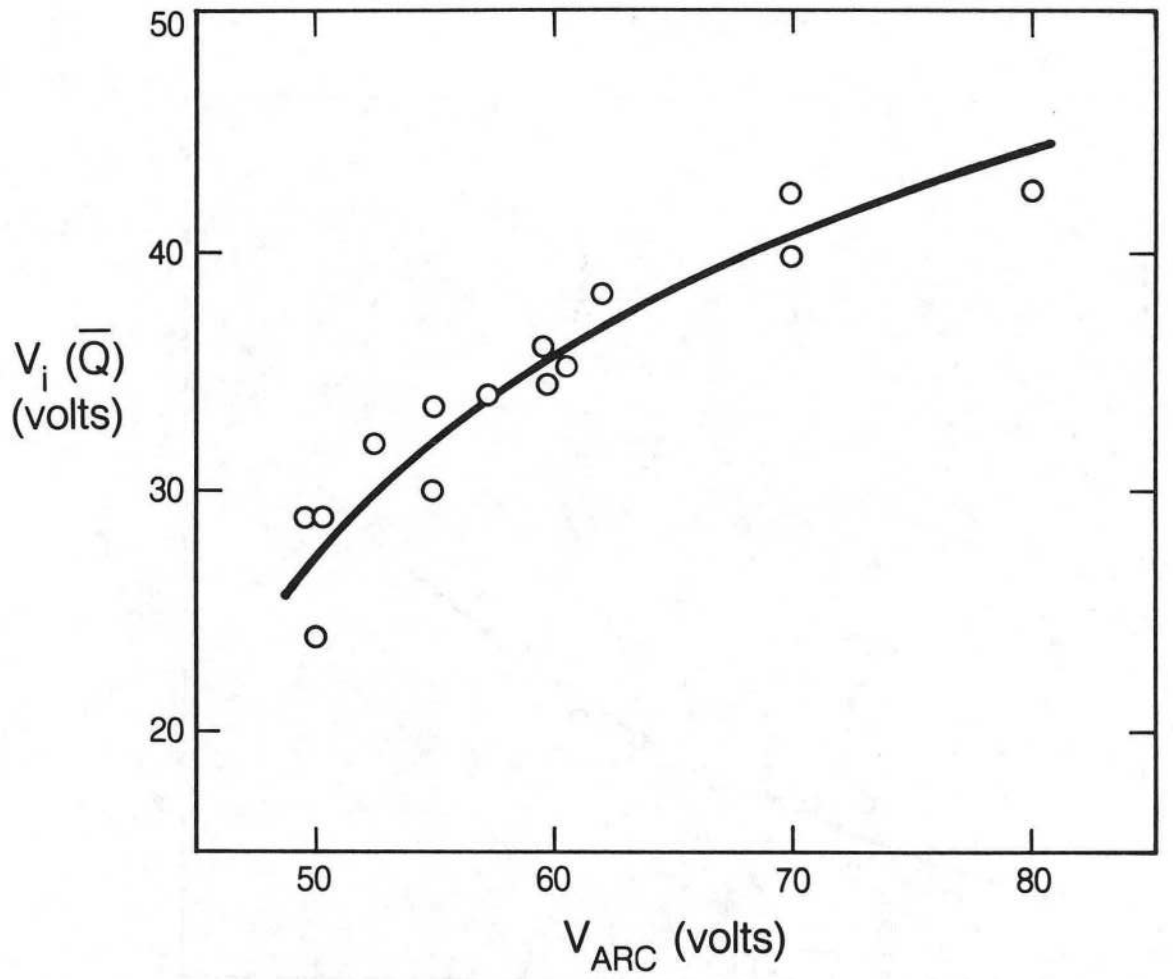

Fig. 16

XBL 854-9940

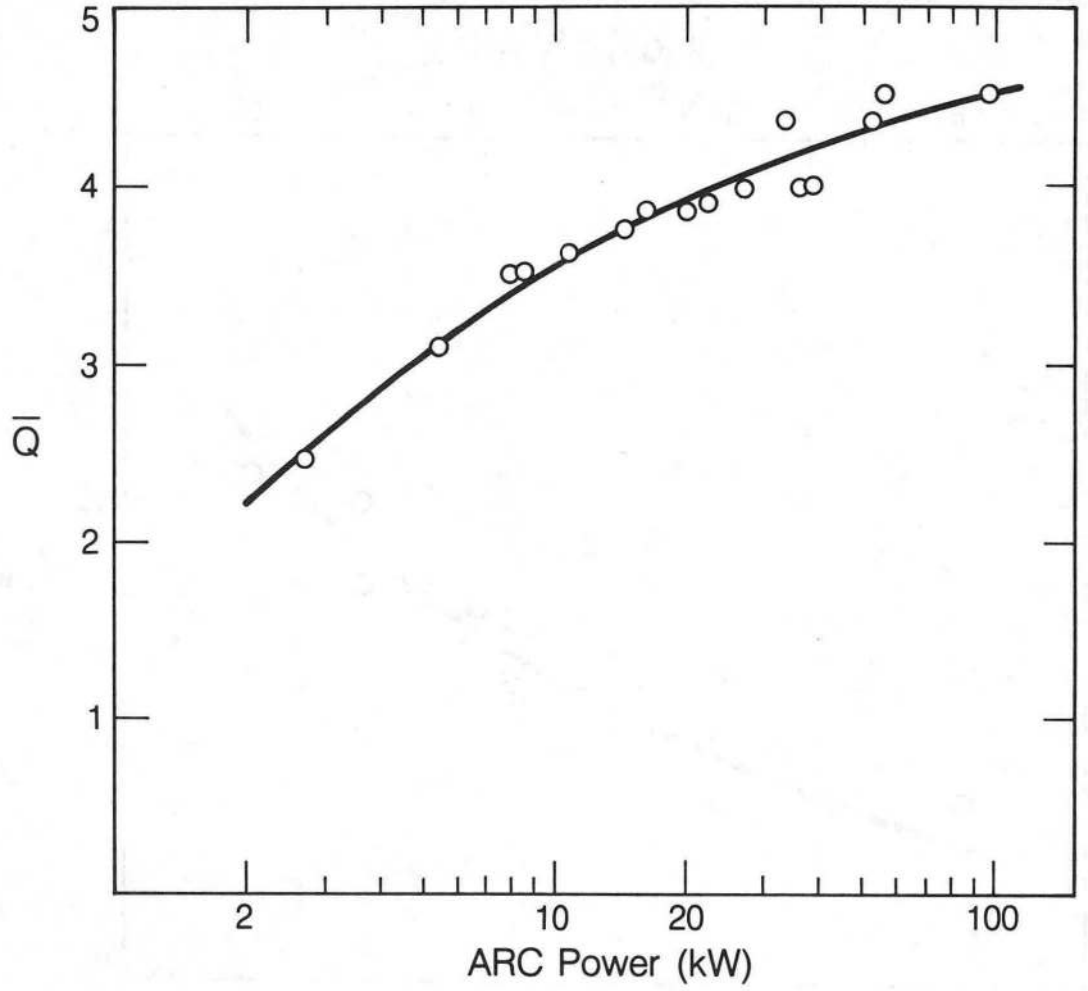

Fig. 17

XBL 854-9941

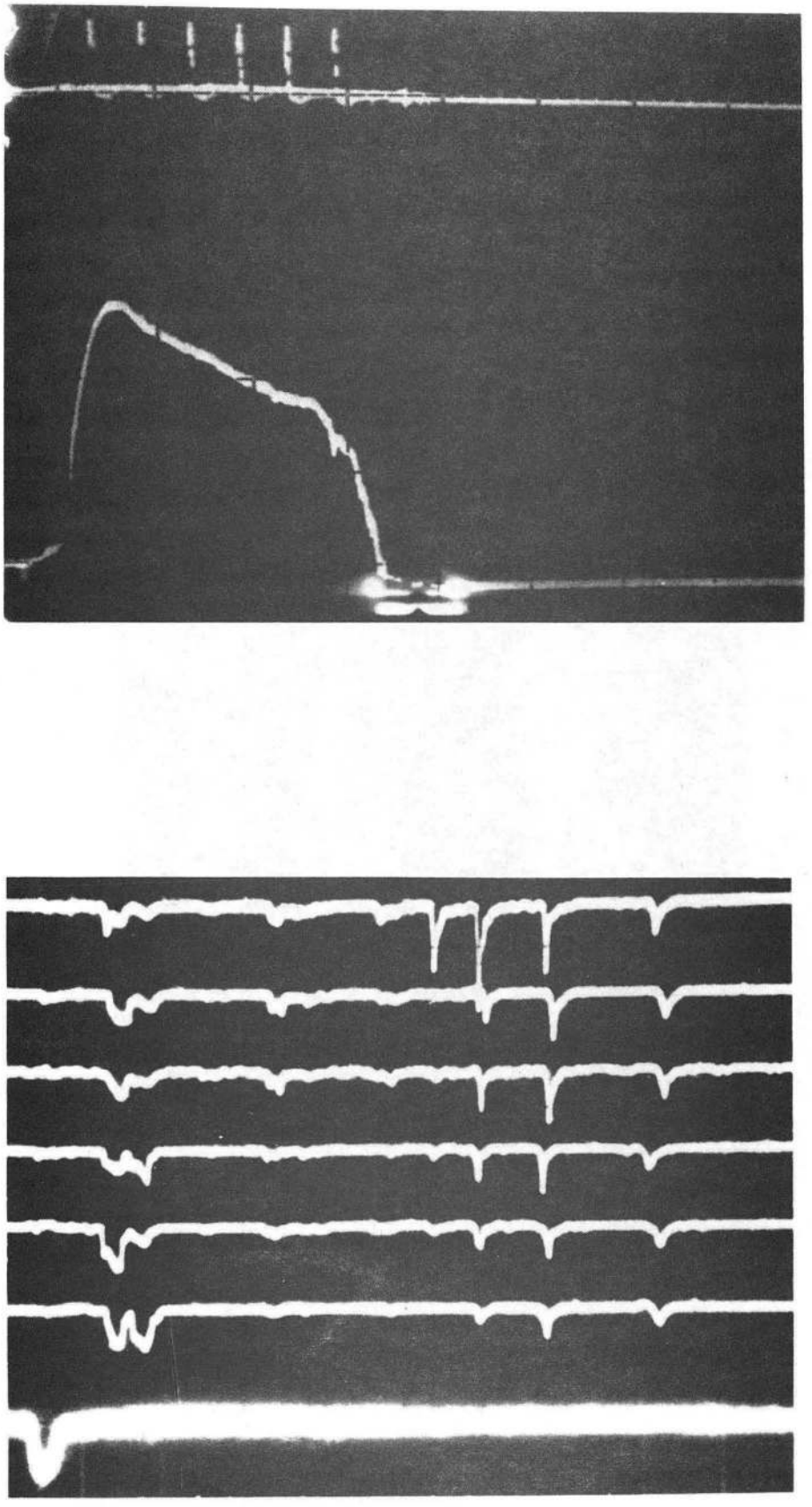

Fig. 18 XBB 854-2877A

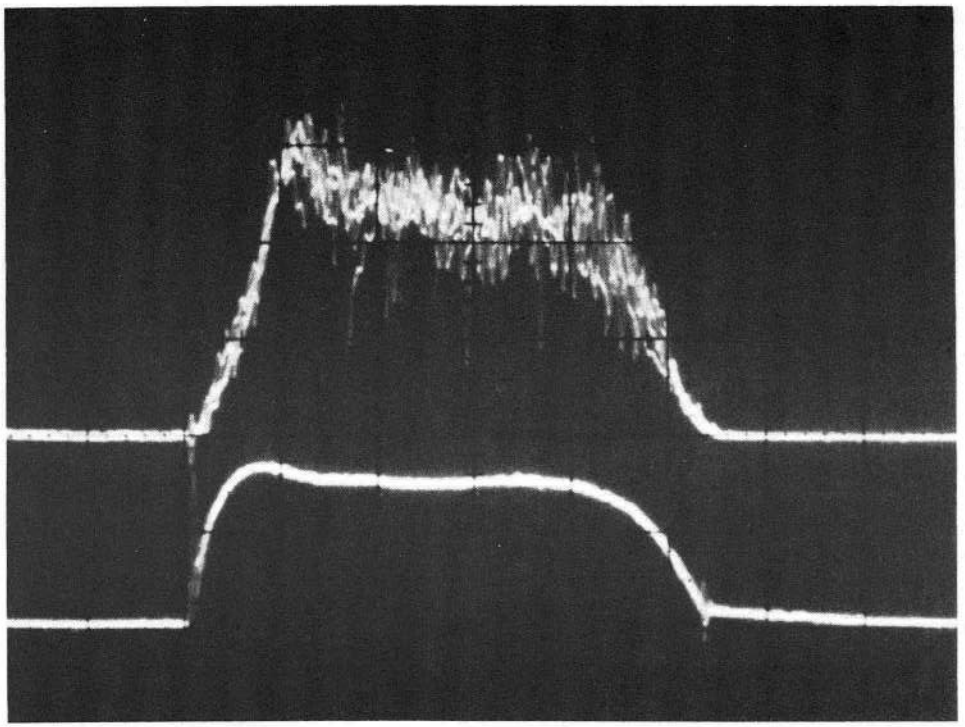

Fig. 19

XBB 858-6534

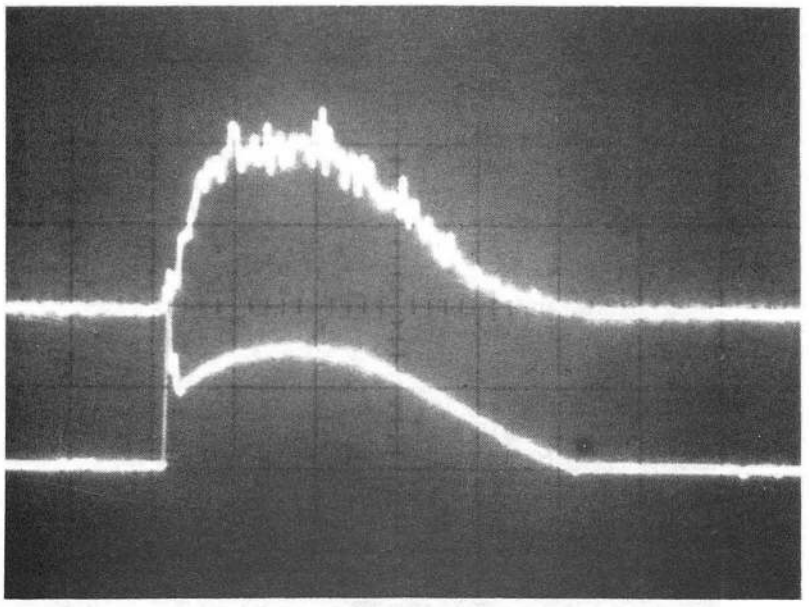

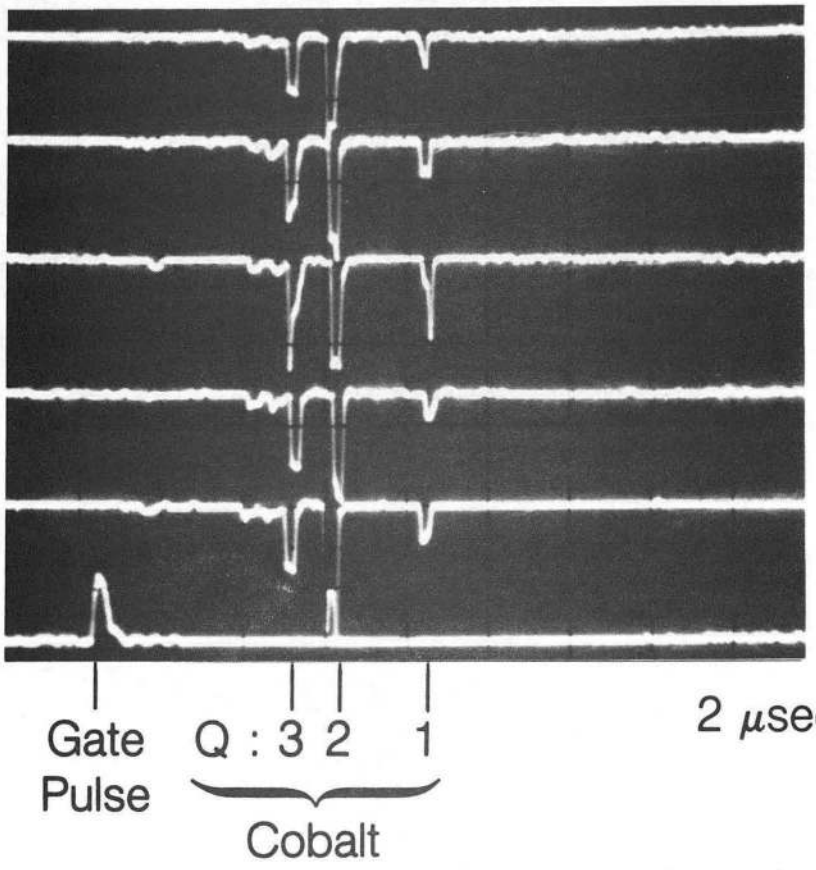

Fig. 20

XBB 858-6323

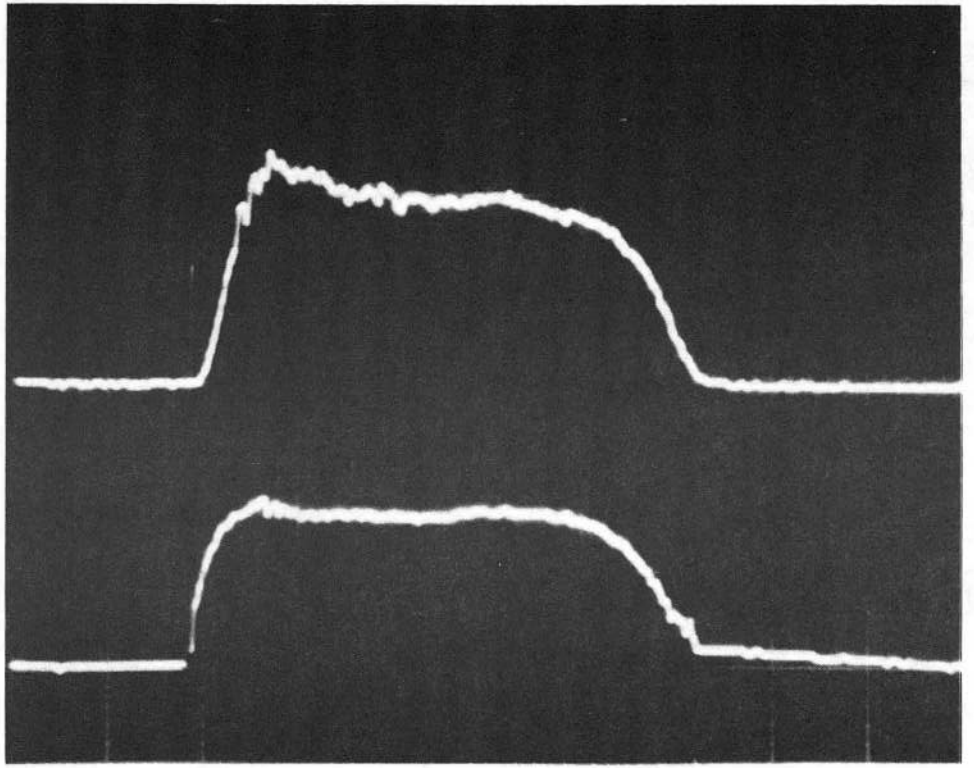

Fig. 21

XBB 858-6733

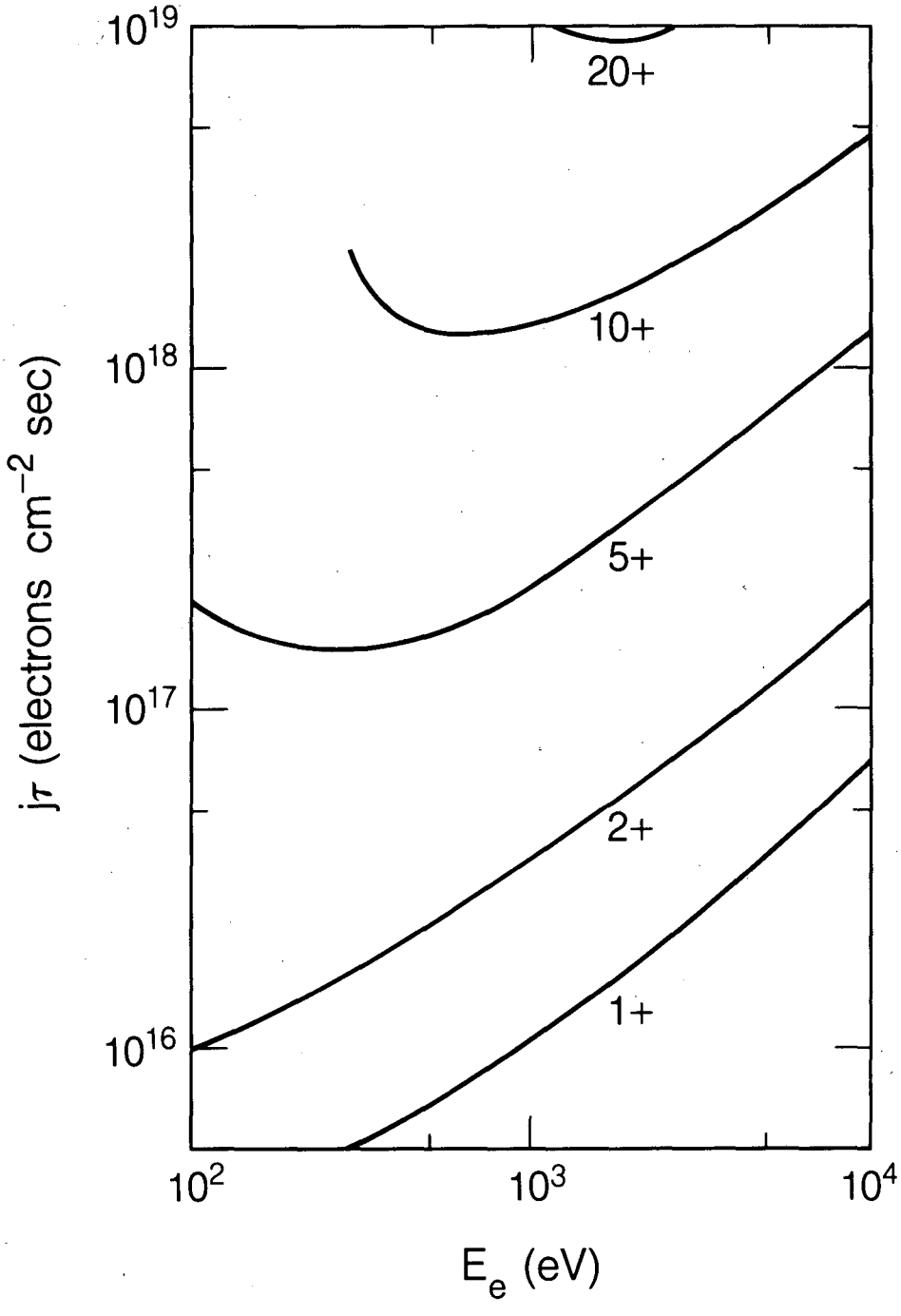

Fig. 22

XBL 858-9879

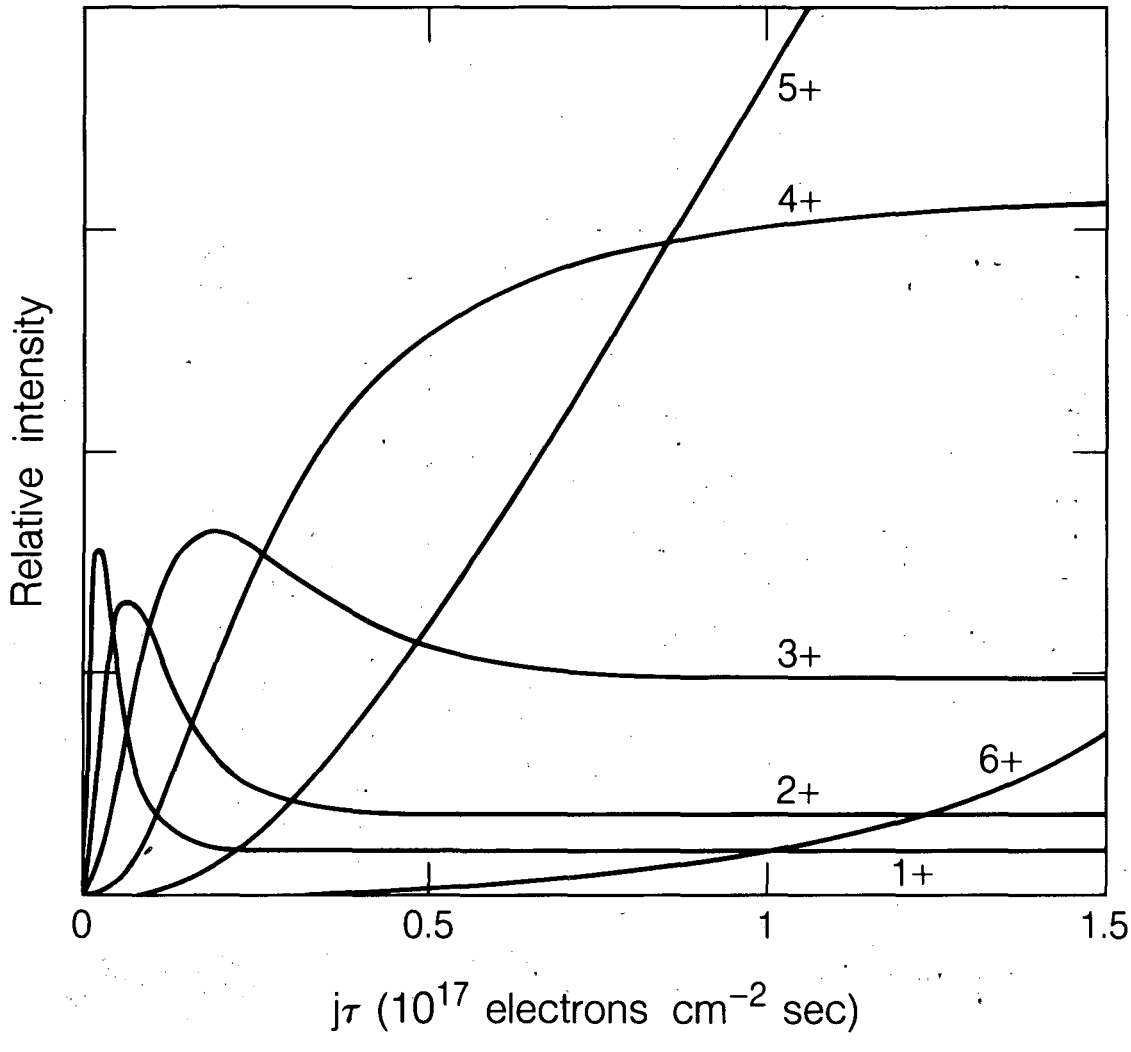

Fig. 23

XBL 858-9874

Q	2	3	4	5	6
Experimental (%)	5	10	35	47	2
Theoretical (%)	5	12	35	46	3

This report was done with support from the Department of Energy. Any conclusions or opinions expressed in this report represent solely those of the author(s) and not necessarily those of The Regents of the University of California, the Lawrence Berkeley Laboratory or the Department of Energy.

Reference to a company or product name does not imply approval or recommendation of the product by the University of California or the U.S. Department of Energy to the exclusion of others that may be suitable.

LAWRENCE BERKELEY LABORATORY
TECHNICAL INFORMATION DEPARTMENT
UNIVERSITY OF CALIFORNIA
BERKELEY, CALIFORNIA 94720